



HAL
open science

Assessing Photoreceptor Status in Retinal Dystrophies: From High-Resolution Imaging to Functional Vision

José-Alain Sahel, Kate Grieve, Chloé Pagot, Colas Authié, Saddek Mohand-Said, Michel Paques, Isabelle Audo, Karine Becker, Anne-Elisabeth Chaumet-Riffaud, Line Azoulay, et al.

► **To cite this version:**

José-Alain Sahel, Kate Grieve, Chloé Pagot, Colas Authié, Saddek Mohand-Said, et al.. Assessing Photoreceptor Status in Retinal Dystrophies: From High-Resolution Imaging to Functional Vision. *American Journal of Ophthalmology*, 2021, 230, pp.12 - 47. 10.1016/j.ajo.2021.04.013 . inserm-03717578

HAL Id: inserm-03717578

<https://inserm.hal.science/inserm-03717578>

Submitted on 8 Jul 2022

HAL is a multi-disciplinary open access archive for the deposit and dissemination of scientific research documents, whether they are published or not. The documents may come from teaching and research institutions in France or abroad, or from public or private research centers.

L'archive ouverte pluridisciplinaire **HAL**, est destinée au dépôt et à la diffusion de documents scientifiques de niveau recherche, publiés ou non, émanant des établissements d'enseignement et de recherche français ou étrangers, des laboratoires publics ou privés.



Assessing Photoreceptor Status in Retinal Dystrophies: From High-Resolution Imaging to Functional Vision

JOSÉ-ALAIN SAHEL, KATE GRIEVE, CHLOÉ PAGOT, COLAS AUTHIÉ, SADDEK MOHAND-SAID, MICHEL PAQUES, ISABELLE AUDO, KARINE BECKER, ANNE-ELISABETH CHAUMET-RIFFAUD, LINE AZOULAY, EMMANUEL GUTMAN, THIERRY LÉVEILLARD, CHRISTINA ZEITZ, SERGE PICAUD, DENIZ DALKARA, AND KATIA MARAZOVA

- **PURPOSE:** To describe the value of integrating phenotype/genotype data, disease staging, and evaluation of functional vision in patient-centered management of retinal dystrophies.
- **METHODS:** (1) Cross-sectional structure-function and retrospective longitudinal studies to assess the correlations between standard fundus autofluorescence (FAF), optical coherence tomography, visual acuity (VA), and perimetry (visual field [VF]) examinations to evaluate photoreceptor functional loss in a cohort of patients with rod-cone dystrophy (RCD); (2) flood-illumination adaptive optics (FIAO) imaging focusing on photoreceptor misalignment and orientation of outer segments; and (3) evaluation of the impact of visual impairment in daily life activities, based on functional (visual and mobility) vision assessment in a naturalistic environment in visually impaired subjects with RCD and subjects treated with Luxturna® for RPE65-related Leber congenital amaurosis before and after therapy.
- **RESULTS:** The results of the cross-sectional transversal study showed that (1) VA and macular sensitivity were weakly correlated with the structural variables; and (2) functional impairment (VF) was correlated with reduction of anatomical markers of photoreceptor structure and increased width of autofluorescent ring. The dimen-

sions of the ring of increased FAF evolved faster. Other criteria that differed among groups were the lengths of the ellipsoid zone, the external limiting membrane, and the foveal thickness. FIAO revealed a variety of phenotypes: paradoxical visibility of foveal cones; heterogeneous brightness of cones; dim, inner segment-like, and RPE-like mosaic. Directional illumination by varying orientation of incident light (Stiles-Crawford effect) and the amount of side illumination (gaze-dependent imaging) affected photoreceptor visibility. Mobility assessment under different lighting conditions showed correlation with VF, VA, contrast sensitivity (CS), and dark adaptation, with different predictive values depending on mobility study paradigms and illumination level. At high illumination level (235 lux), VF was a predictor for all mobility performance models. Under low illumination (1 and 2 lux), VF was the most significant predictor of mobility performance variables, while CS best explained the number of collisions and segments. In subjects treated with Luxturna®, a very favorable impact on travel speed and reduction in the number of collisions, especially at low luminance, was observable 6 months following injection, in both children and adults.

- **CONCLUSIONS:** Our results suggest the benefit of development and implementation of quantitative and reproducible tools to evaluate the status of photoreceptors and the impact of both visual impairment and novel therapies in real-life conditions. **NOTE:** Publication of this article is sponsored by the American Ophthalmological Society. (Am J Ophthalmol 2021;230: 12–47. © 2021 The Authors. Published by Elsevier Inc. This is an open access article under the CC BY-NC-ND license (<http://creativecommons.org/licenses/by-nc-nd/4.0/>))

Accepted for publication April 15, 2021.

From the Department of Ophthalmology, University of Pittsburgh School of Medicine and Medical Center, Pittsburgh, Pennsylvania, USA (J.-A.S.); Sorbonne Université, Paris, France (J.-A.S.); Quinze Vingts National Ophthalmology Hospital, Paris, France (J.A.S., K.G., S.M.-S., M.P., I.A., A.-E.C.-R., L.A.); StreetLab - Institut de la Vision, Paris, France (C.P., C.A., K.B., E.G.); and Institut de la Vision, Sorbonne Université, Inserm, CNRS Paris, France (M.P., I.A., T.L., C.Z., S.P., D.D., K.M.).

Inquiries to José-Alain Sahel, Department of Ophthalmology, University of Pittsburgh School of Medicine and Medical Center, 203 Lothrop St, Suite 817, Pittsburgh, PA 15213, USA / Institut de la Vision, 17 rue Moreau, 75012 Paris, France; e-mail: sahelja@upmc.edu, j.sahel@gmail.com

OVERVIEW

• **INHERITED AND AGE-RELATED RETINAL DEGENERATIVE DISEASES: CONTRIBUTION TO THE OVERALL BURDEN OF VISUAL IMPAIRMENT:** Inherited and age-related retinal degenerative diseases are a major cause of untreatable blindness. Characterized by progressive photoreceptor degeneration, inherited retinal dystrophies (IRDs), a large group of Mendelian or mitochondrially inherited disorders, are characterized by extensive genetic and phenotypic heterogeneity. Profound vision loss and blindness are a common occurrence in these pathologies, not infrequently from birth or early childhood. Obviously, the devastating health and socioeconomic consequences of visual impairment call for novel and efficient strategies for preserving or restoring vision. The first mutations reported in the human rhodopsin gene in 1990 in patients with autosomal dominant retinitis pigmentosa (RP), also called rod-cone dystrophy,¹ identified through linkage studies and DNA sequence analysis, raised hopes in scientists and patients about future therapies to cure retinal blindness. Indeed, since then, vision research and ophthalmology have seen a notable success of using gene replacement strategies for blinding retinal disease. The past decade has witnessed the emergence of numerous strategies for preserving or restoring some sight in these conditions. A new era in the perspectives for vision therapies began with the recent approval of the gene therapy product Luxturna® for treatment of RPE65-associated Leber congenital amaurosis (LCA). The market authorization of the first-ever gene therapy for LCA, the most severe IRD,² signals the culmination of decades of research on genetics and mechanisms of vision loss, animal models, vector design, imaging, and microsurgery.

Today, vision research witnesses an unprecedented increase in the number of gene therapy trials, cell therapy, and prosthetic vision. At this pivotal time of real-life implementation of the biotechnological advancements for saving sight, the expectations of both patients and the public are growing.

Here we describe our experience in developing and testing novel strategies for vision preservation/restoration in IRDs, with a special focus on the identification of patients that would benefit most from each approach and on demonstration of the real-life benefit. We intend to demonstrate the value of a holistic approach integrating not only structural and functional markers of disease progression and potential rescue, but also the impact of disease and potential therapies on functional vision, thus better reflecting patient experience. The latter may require the development of qualitative research concepts and methods that fall beyond the scope of this work. This thesis will first describe some of the clinical technologies used to assess the status of retinal photoreceptors as a prerequisite for therapeutic decision-making and for the assessment of treatment efficiency. We

will then focus on the development and validation of quantitative and reproducible tools to assess the impact of both visual impairment and novel therapies in daily life.

• **WHY A PERSONALIZED APPROACH BASED ON BOTH GENOTYPIC AND PHENOTYPIC PRESENTATION MATTERS: MUTATION-SPECIFIC AND MUTATION-INDEPENDENT THERAPEUTIC APPROACHES:** The emergence of gene therapy, including both gene supplementation and gene editing, as well as the antisense oligonucleotide approach targeting the mutated messenger RNA, puts a strong focus on the assessment of the status of photoreceptors, both rods and cones, in order to determine the existence and number of cells to be targeted, as well as their viability. At more advanced stages of the disease process, the protection of remaining cones is a gene-independent approach. Assessing the status of cone photoreceptors is required before and following therapy. In retinas where cones have lost outer segments and are considered dormant, reactivation by optogenetics can restore some visual function. Finally, replacement approaches can be envisioned at stages where only inner retinal cells are present.³⁻⁵ The assessment of retinal structure is a key element in decision-making, besides the genetic cause of the disease, and should be considered as part of a personalized medicine approach.

• **ASSESSMENT OF DISEASE STAGE AND VISUAL FUNCTION IN PATIENTS WITH INHERITED RETINAL DYSTROPHIES BEFORE AND AFTER TREATMENT:** Selection of patients that might benefit from the emerging therapies (i.e., gene therapy, neuroprotection, optogenetics, retinal prosthesis) is the first step toward therapeutic success. The choice of therapy will depend on the disease stage, and especially on the status of photoreceptors that will be assessed through a carefully designed battery of relevant tests (Figure 1). The demonstration of the impact of the therapy on functional vision is essential. Appropriate outcome measures for evaluating the efficiency of the treatment is another key element in the pathway toward novel therapies to save vision (reviewed in ⁶).

The remarkable invention of the ophthalmoscope 170 years ago by an outstanding physicist, Hermann von Helmholtz, allowed the first observation of human eye fundus. As the retina consists of a dozen layers of mostly transparent tissue, however, it cannot be directly observed in the living eye. This became possible with the discovery and introduction to the ophthalmology practice of optical coherence tomography (OCT) and adaptive optics (AO)-enhanced ophthalmoscopy (AOO) in the 1990s. Today, OCT is routinely used in ophthalmology, while AOO is now consistently used predominantly for science observations and clinical research. While OCT's axial resolution permits visualization of the retina's laminar structure and identification of the different neuronal layers, AOO gives optical access to individual retinal cells (e.g., rod and cone photoreceptors, retinal pigment epithelium [RPE] cells)

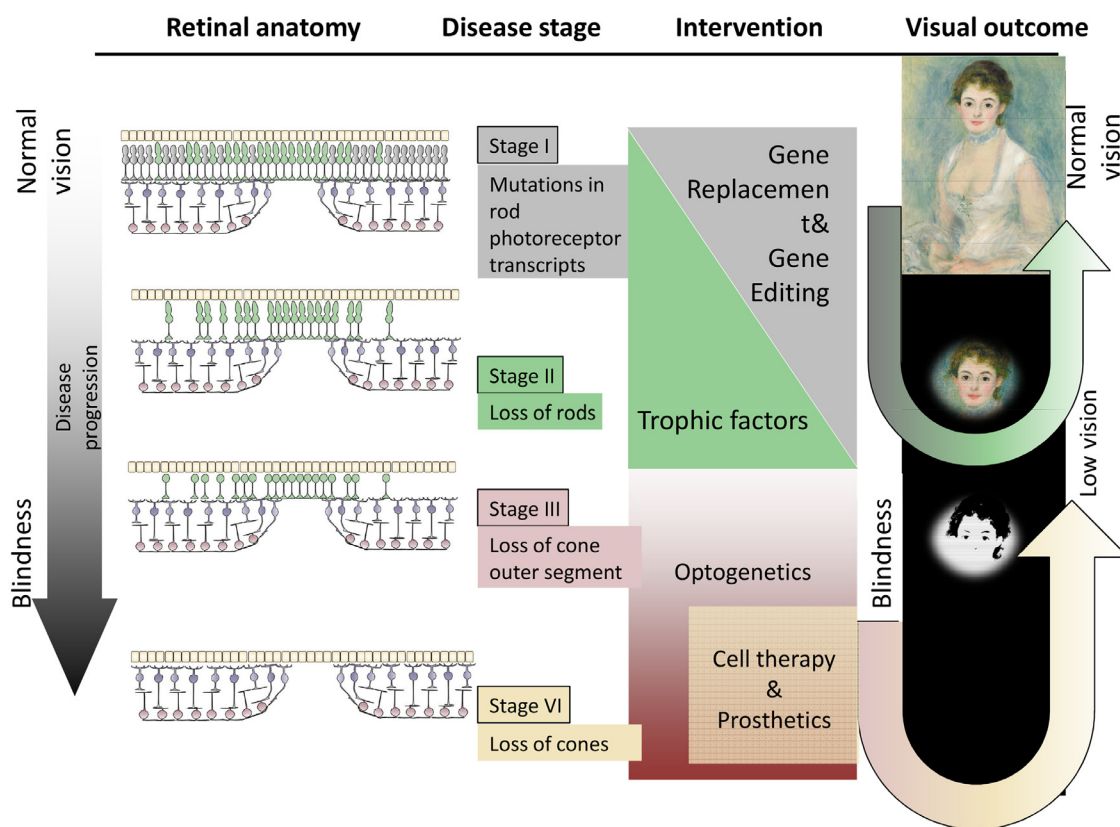


FIGURE 1. Gene replacement therapy is appropriate during the early stages of disease, when retinal photoreceptor cells are still intact. Early intervention with gene replacement, gene editing, or antisense oligonucleotides can potentially reverse vision loss and lead to close to normal visual outcomes. Neuroprotective strategies, particularly those targeted to preserve cones, are the best approaches to treat the disease with ongoing photoreceptor cell degeneration. Cone neuroprotection can stave off loss of high-acuity vision by protecting foveal cones. Stem cell therapy, optogenetic therapy, and retinal prostheses are used to restore vision during the later stages of retinal degeneration, after the loss of cone outer segments. These approaches can be applied independently from the causal mutation and are expected to restore low vision in blind patients. [From *Sci Transl Med* 2019;11(494):eaax2324. doi: 10.1126/scitranslmed.aax2324. (Courtesy of Dalkara D).]

in the living human eye. These two noninvasive optical technologies along with fundus autofluorescence imaging that has important diagnostic value carry huge diagnostic, monitoring, and prognostic potential for IRDs and age-related retinal diseases and are objects of continued development for providing better *in vivo* views of the normal and diseased retina.

RP is characterized by a long-term degenerative process of rods that secondarily affects cones. The whole retinal structure, including the extracellular matrix, retinal pigment epithelium cells and vessels may also be affected in later stages. As opposed to other diseases such as geographic atrophy, RP is characterized by a smooth transition from the healthy to the degenerated tissue; hence, the limits of the degenerated area show a progressive loss of contrast. Additionally, since the rods are in most cases lost at first diagnosis, there is necessarily alteration of the extracellular milieu of central cones; hence, there are already changes of the light-tissue interactions around cones. Therefore, the process observed by *in vivo* imaging is essentially that of

the secondary degeneration of cones. Finally, other disease processes such as pigment dispersion, misalignment of outer segments and cysts, or media opacities such as cataract may further alter fundus imaging.

The optical properties of the retina may thereby be affected in a number of ways, and the limit between the affected and unaffected retina is often difficult to determine. This represents both a challenge and an opportunity for the development of imaging technologies and protocols.

Morphologic and functional integrity of the cone photoreceptors is of utmost importance for ensuring daytime, detailed, and color vision. Since the initial observations of living cone photoreceptors,^{7,8} the density and the directionality/orientation of the retinal cones (determined by the waveguide properties of the cones and the topography of the cone mosaic) have been the object of considerable interest. Cones are more sensitive to light entering via the center of the pupil than via its periphery.⁹ This directional sensitivity of the cone photoreceptors defines the Stiles-Crawford effect (reviewed in¹⁰). In line with the increasing

body of evidence demonstrating alteration in the cone density and presence of photoreceptor disarray in a variety of retinal diseases, we focused our investigations toward detecting photoreceptor misalignment and unveiling the role of the directional variability in healthy and diseased retina. Cone photoreceptor length and the thickness of intraretinal layers can be measured by spectral-domain OCT. When the OCT technology is extended to acquire sets of images taken at different points of penetration through the pupil (ie, multiangle, directional OCT¹¹), it reveals the reflectance properties of the photoreceptor substructures, permitting evaluation of the cone orientation and directionally sensitive structures (such as the inner/outer segment limit) that can be used as biomarkers of retinal diseases.

Adaptive optics-enhanced ophthalmoscopy systems are either scan- or flood-based. Compared to scan-based imaging devices, flood-illumination systems have received much less attention from the scientific community despite several technical advantages. The most obvious of these advantages is the fact that there is no image distortion; thus, flood-based AO fundus cameras are now increasingly recognized as providing a “ground truth” of fundus features, over which scan-based images may be registered.¹² The fact that the flood AO cameras lack the optical sectioning of confocal AO scanning laser ophthalmoscope systems reduces contrast on specific layers, yet ensures that uneven fundus can be correctly imaged. Larger fields of view can be obtained by flood AO (typically 4 degrees vs 2 degrees). Flood-based systems also provide contrast on additional features such as melanin deposition. Finally, evaluating the effect of light incidence and hence determining the orientation of outer segments can be done more conveniently on flood systems than on scan systems. To our knowledge, there has been no extensive review of flood AO fundus imaging in RP patients.

• **WHY WE NEED TO MEASURE FUNCTIONAL VISION:** Translational programs are now underway at many pharmaceutical corporations, biotechnology companies, and academic institutions around the world. They often target people who have lost their vision owing to genetic or age-related diseases and who could be the earliest candidates to receive any of the emerging vision restoration strategies, including gene therapy, cell therapy, optogenetics, and visual prosthesis. Relevant measurements and tests to quantify vision before and after treatment are mandatory, as is the objective evaluation of the therapeutic benefit for patients.

“Functional vision” is often described as the ability to independently conduct vision-dependent tasks that are essential for maintaining activities of daily life. The assessment of functional vision in people with ultra-low vision or complete blindness represents a major challenge to the translation of research discoveries to the clinic. In addition to evaluating “classical” specific outcomes reflecting visual function, such as visual acuity (VA), contrast sensitivity (CS), and visual field (VF), translational

researchers focused on the development of outcomes evaluating the visual improvement for multiple tasks of daily life, such as orientation, mobility, and reading, known as performance-based tests.

Early experience from clinical trials with emerging vision restoration therapies called for development of novel testing methods and reliable measures for assessment of functional vision. In the Argus II clinical trial, the retinal prosthesis was implanted in people with severe visual impairment in both eyes (bare light perception or worse, >2.9 logMAR).¹³ Standard clinical charts such the Early Treatment Diabetic Retinopathy Study (ETDRS) chart that can measure acuity down to levels of logMAR 1.60 (20/800 or 6/240) were not applicable for these patients. Post intervention, even the best-performing implanted subjects did not achieve this level of acuity or did not improve to the level of “legal blindness”; thus, it was impossible to measure the treatment benefit through this and other routinely used visual assessments. To determine the treatment efficacy, the Argus II trial introduced custom-designed assessments, named “Square Localization,” “Direction of Motion,” and “Grating Visual Acuity,” all of them performed on a computer monitor, and “Door Task” and “Line Task” real-world assessments, together with Vision-related Quality of Life questionnaires.¹³ In 2013 the U.S. Food and Drug Administration (FDA) provided specific recommendations on the validation of such technologies, emphasizing the value of patient-reported outcomes and of functional vision assessment (Investigational Device Exemption [IDE] Guidance for Retinal Prostheses / Guidance for Industry and Food and Drug Administration Staff; <https://www.fda.gov/media/85270/download>). Retina Implant AG also developed a subretinal prosthesis that provided some functional benefit in terms of formed vision, but the device was discontinued before approval was sought.

Such an innovative approach to measure functional vision was also strikingly brought into practice by the clinical trial evaluating the safety and efficacy of gene therapy (AAV2-hRPE65v2) in patients with RPE65-LCA. In response to the need for a relevant, reliable, and clinically meaningful measure of functional vision in the study participants with nyctalopia, the study team, with input from the FDA, developed and introduced a standardized multiluminance mobility test allowing for tracking functional vision changes at specified light levels over time in low-vision patients (VA of 20/60 or worse).^{2,14}

Over the past 10 years, to address the need of measuring functional vision, we have developed and built a low vision rehabilitation center dedicated to new methods of evaluation and training. This center is committed to evaluate therapeutic benefits and innovative solutions for mobility in real-life conditions. In addition, it aims to create a supportive environment for comprehensive investigation of behavioral and adaptive mechanisms in visually impaired patients. This center, named StreetLab, comprises 3



FIGURE 2. View of the “Streetlab” artificial street.

evaluation platforms: an artificial street (Streetlab), a test apartment (Homelab), and a driving simulator.

The “Streetlab” artificial street represents an indoor platform conceived to reproduce an urban environment with realistic and immersive street elements with dimensions of 9 m length, 7 m width, and 5.5 m height (Figure 2). Modular lighting and homogeneous light distribution is ensured by 9 light panels of 3.5 m² each. The light intensity and the color temperature are configurable (0-2,000 lux / 2,700-6,500 k). A 3-D sound system allows for simulation (homogeneously diffused or triggered) of street auditory impacts through audio recordings of urban soundscapes. The fully controlled Streetlab conditions can be tailored to the needs of different experiments in terms of light, sound, and adjustable scenery (decoration, furnishing, color scheme, etc.) and are associated with objective motion-capture measurement systems to record human movements. The reproducibility of the experimental conditions is ensured by integrated measurement tools (eye-tracker, Vicon motion capture system with passive markers, inertial sensors) and fully controlled auditory and visual immersion systems (adjustable scenery, control of the light intensity and color). Monitoring and 3-D video recording through surveillance cameras, and processing of the collected information using Python software, constitute an essential part of the evaluation procedures in the artificial street. VICON Motion Systems Inc., Los Angeles, 8 cameras, 120 Hz; Python (Python 2.7.6, www.python.org).

All parameters are variable and can be set and modified remotely from a control room (Figure 3).

Several studies were performed in this platform. They allowed us to demonstrate that the precise evaluation of

the ability of glaucoma patients to perform everyday life tasks is complex and may require both monocular and binocular VF tests.¹⁵ Also, in glaucoma patients, not only is the quality of life altered but also their ability to perform common activities of daily life.¹⁶ In Streetlab, we identified novel indicators of postural control interfering with spatial learning and navigation capabilities in the elderly, and we tested the hypothesis that navigation difficulties in elderly people are associated with deficits in processing and encoding spatial cues.^{17,18} We also evaluated the age-related differences in functional and structural connectivity of spatial navigation.^{19,20} Here, we shall report elements of our experience in the field of IRDs.

Here, we report on novel in vivo high-resolution imaging methods that can assist disease staging and will help in evaluating treatment efficiency (i.e., by evaluating rescue of photoreceptor structure and function); and we offer an overview of the concept, development, validation, and achievements of the innovative Streetlab platform, dedicated to assessing the real-life benefit of neuroprotection and optogenetic therapies for patients with retinal degenerative diseases.

METHODS

• **CROSS-SECTIONAL STRUCTURE-FUNCTION CORRELATION STUDY:** We performed a transversal structure-function correlation study and a retrospective longitudinal study in a large cohort of patients affected with rod-cone dystrophy. The objective of this work was to study the



FIGURE 3. View of the “Streetlab” control room.

correlations between the different variables measured from standard fundus autofluorescence and OCT examinations, and functional data including VA and static perimetry, to highlight the structural severity criteria that predicted an important level of functional loss.

The study population consisted of 172 adult patients with RP (rod-cone dystrophy) without any other ocular or general complication or disease, selected from the cohort followed at the Rare Disease Reference Centre of the Quinze Vingts National Ophthalmology Hospital, and a group of 15 age-matched healthy controls.

Functional data collected and analyzed were best-corrected VA, central sensitivity, and mean sensitivity extracted from static perimetry.

Structural data

Fundus autofluorescence (FAF) imaging pictures were acquired with the Heidelberg retina angiograph (HRA2; Heidelberg Engineering, Heidelberg, Germany). We measured the dimensions of the ring of increased autofluorescence in the macular region. The parameters analyzed were (Figure 4):

- Surface of the area delimited by the internal edge of the ring (mm^2) = FAF_ACI
- Surface of the ring of hyper-autofluorescence (mm^2) = FAF_area-HAF
- Horizontal diameter of the internal edge of the ring (μm) = FAF_GAH
- Horizontal width of the ring of hyper-autofluorescence (μm) = FAF_HAFh
- Vertical diameter of the internal edge of the ring (μm) = FAF_GAV

- Vertical width of the ring of hyper-autofluorescence (μm) = FAF_HAFv

OCT data were obtained from Heidelberg Spectralis (Figure 5). We measured the length of preserved ellipsoid zone (OCT-EZh and OCT-EZv) and the external limiting membrane (OCT-ELMh and OCT-ELMv) on the horizontal and vertical scans. The retinal thickness was extracted from the 20-degree volume scan (Figure 6):

- OCT_Ep_0-1: Average thickness of the retina within the 1 mm around the fovea
- OCT_Ep_1-3: Average thickness of the retina located between 1 and 3 mm from the fovea
- OCT_Ep_3-6: Average thickness of the retina located between 3 and 6 mm from the fovea
- OCT_Volg: Retinal average volume within the 6 mm circle around the fovea.

First, we analyzed the correlations between the functional and structural variables to determine the severity criteria related to the greatest functional deterioration (measured by VA and mean macular sensitivity [MS]) for each structural variable. In a second step, we included the patients in different groups according to their functional impairment to determine whether a functional impairment is related to significantly different values of the structural variables. We analyzed these correlations in 3 groups according to the VA level:

- $VA \leq 0.3$ (Monnoyer) corresponding to 20/63 Snellen ($n = 23$);
- $0.3 < VA \leq 0.7$ - 20/63-20/25 ($n = 64$);
- $VA > 0.7$ - 20/25 ($n = 82$)

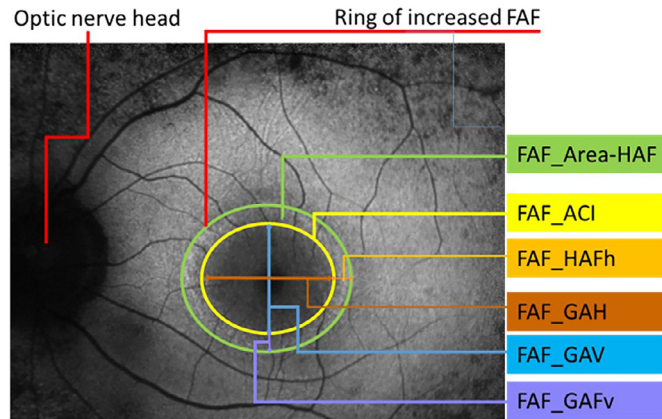


FIGURE 4. Fundus autofluorescence picture of a retinitis pigmentosa (RP) patient with a ring of increased autofluorescence and the respective measured parameters.

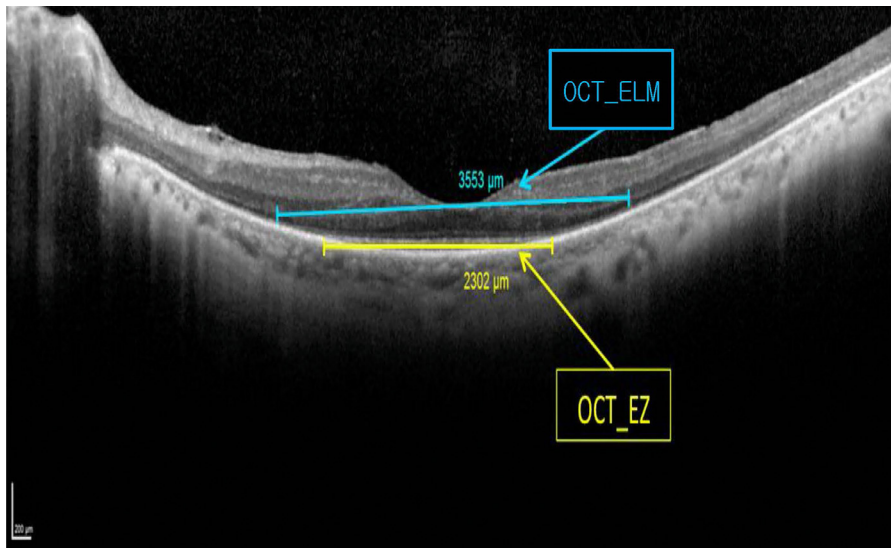


FIGURE 5. Ellipsoid zone and external limiting membrane measured on the horizontal scan of the left eye of a retinitis pigmentosa patient.

and according to the level of mean MS:

- MS \leq 10 dB (n = 49);
- 10 dB < MS \leq 20 dB (n = 78);
- MS > 20 dB (n = 45).

• **HIGH-RESOLUTION ADAPTIVE OPTICS RETINAL IMAGING:** Flood-illumination AO images from 10 eyes of 10 patients with rod-cone dystrophies were acquired and reviewed. Patients were included in a clinical trial on retinal imaging (registered in clinicaltrials.gov NCT01546181). This institutional clinical study was carried out according to the principles outlined in the Declaration of Helsinki. Approval of the ethics committee of Saint-Antoine Hospital (Paris, France) was obtained. Patients with rod-cone dystrophies from various genetic causes were examined.

The image protocol was as follows: Flood-illumination adaptive optics (FIAO) imaging was performed with a commercially available FIAO camera (rtx1; Imagine Eyes, Orsay, France). The adaptive optics loop features a 750 nm superluminescent diode beam to measure the point spread function by a Shack-Hartmann wavefront sensor (40 × 32 array). Correction is performed via a deformable mirror (Mirao 52e; Imagine Eyes, Orsay, France). The imaging path comprises an 850 nm flood illumination by light-emitting diode (LED) creating a uniform 4 × 4 degree field on the retina, whose reflection is captured by a 656 × 494 pixel charge-coupled device camera.

The fundus imaging procedure is briefly summarized hereafter. En face FIAO fundus images were obtained through fully dilated pupils (1% tropicamide; Novartis, Rueil Malmaison, France) in light adapted, unbleached eyes. During examination, two live screen images are displayed: one showing the AO corrected fundus image,

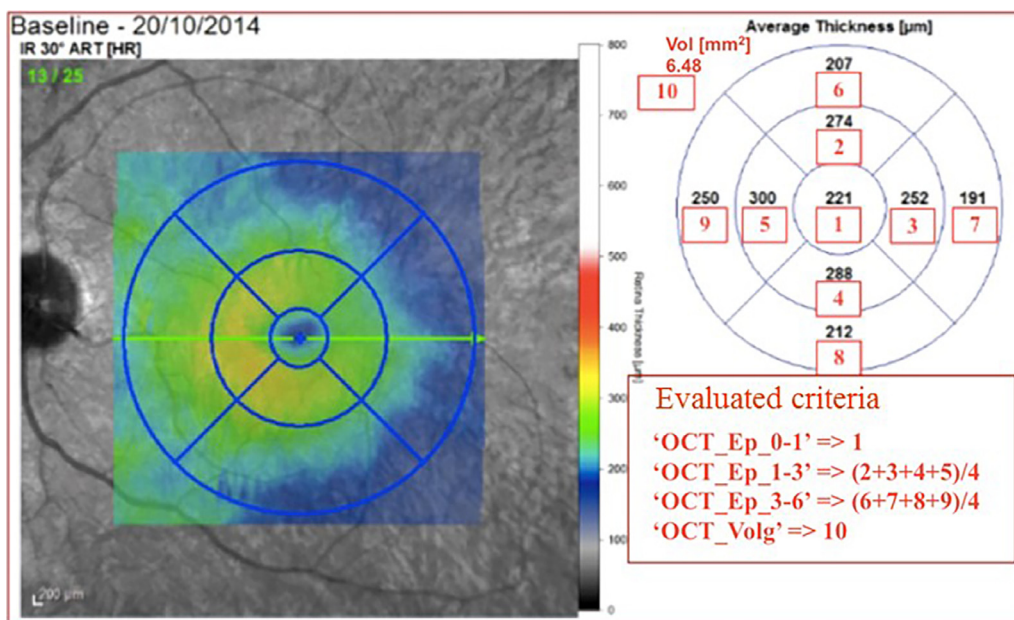


FIGURE 6. Optical coherence tomography parameters analyzed in retinitis pigmentosa and control groups.

and the other the corneal reflection (first Purkinje image) of four LED sources together with the center of the entry beam. To acquire images at different incidences, the entry pupil was manually shifted in one of the cardinal directions while observing the corneal reflection, and another image of the same region was acquired. Shifting of the joystick was done while checking the live retinal image to ensure that patches of cones remained visible in the live image. On average, a 2.6-degree offset was thus obtained; however, the amount of shifting varied significantly between images (typically from 0.5 to 3 degrees). Gaze variability was analyzed by comparing the intersection of overlapping images; any difference between the two images is possibly related to the balance between the on-axis reflected and the multiply backscattered light; that is, structures on the side of the image receive proportionally more multiply backscattered light than structures in the center of the field of view.

Each stack of 40 raw images acquired in 2 seconds by the AO camera was processed using the built-in software. Raw images were registered and averaged to produce a final image with improved signal-to-noise ratio; the background of the resulting image was subtracted using a Gaussian filter and the histogram was stretched over a 16-bit range of gray levels. Images taken at different entry pupils were registered by rotation and size adjustment using either Adobe Photoshop 7.0 (Adobe Corporation, Mountain View, California, USA) or i2k Align Retina software (DualAlign, LLC, Clifton Park, New York, USA) in combination. The effect of gaze orientation was analyzed by calculating the standard deviation of the ImageJ Z projection plugin (available in the public domain at rsb.info.nih.gov/ij/; National Institutes of Health, Bethesda, Maryland, USA).

• **ASSESSING FUNCTIONAL VISION:** We report in this paper two case studies that assess functional vision in IRDs: (1) assessing mobility in visually impaired subjects with RP; and (2) assessing mobility in subjects treated with Luxturna[®] for RPE65-LCA.

Subjects

First case study: Assessing mobility in visually impaired subjects with retinitis pigmentosa. A prospective study included 17 visually impaired subjects with RP and 10 fully sighted control subjects (CO) recruited at the Quinze Vingts National Ophthalmology Hospital in Paris, France. The study was conducted according to the principles of the Declaration of Helsinki and approved by an ethics committee (Comité De Protection Des Personnes Ile –De–France (CPP) V, Paris, n° EudraCT: 2015-003400-24). Informed written consent was obtained from all participants.

The RP inclusion criteria were clinical diagnosis of RP confirmed by visual assessment and retinal electrophysiology, binocular VF <40 degrees, and VA \leq +0.3 logMAR. The CO inclusion criteria were VA \leq +0.1 logMAR and normal VF. Both groups included subjects aged between 18 and 70 years. Subjects with other neurodegenerative diseases, physical disability, and any other condition or treatment that may impair walking and interfere with the mobility evaluation were not included.

Second case study: Assessing mobility in subjects treated with Luxturna[®] for RPE65-LCA. A retrospective study included 8 visually impaired subjects with RP treated with subretinal injections of voretigene neparvec (Luxturna[®]), according to the indication of the therapy, who underwent mobility assessment. This group included

TABLE 1. Study Population and Visual Tests

Parameters	RP N = 17 Median [Q1; Q3]	CO N = 10 Median [Q1; Q3]	RP vs CO P value
Age at inclusion (y)	46 [33.0; 58.0]	51[39.0; 53.8]	.5
Age at diagnosis (y)	29 [10; 30] 5 missing data		
Visual acuity (logMAR)	0.2 [0.08; 0.3]	-0.2 [-0.2; -0.1]	<.0001
Contrast sensitivity (logCS)	1.80 [1.35; 1.95]	1.95 [1.95; 1.95]	<.001
Horizontal visual field (degrees)	22.2 [11.1; 26.1]	171.5 [166.2; 174.0]	<.0001
Dark adaptometry 1' (dB)	25 [22.8; 30.4]	37.5 [37.2; 38.6]	<.0001
Dark adaptometry 10' (dB)	24.8 [23.9; 42.5]	52.8 [51.7; 54.5]	<.0001

CO = control; RP = retinitis pigmentosa.

3 children (average age 11 ± 2 years) and 5 adults (average age 26 ± 5 years). Each eye was injected 1 week apart.

The inclusion criteria were visual loss owing to inherited retinal dystrophy resulting from confirmed biallelic mutations in the *RPE65* gene; and presence of viable retinal cells in sufficient quantity (as determined by OCT). Patients had to have at least one of the following criteria: retinal thickness $>100 \mu\text{m}$ as measured by OCT at the posterior pole, or presence of ≥ 3 optical disc surface with no area of atrophy, or pigment degeneration at the posterior pole, or maintenance of the VF within 30 degrees of the fixation point measured by isopter III-4e or equivalent.

Study design

First case study: Assessing mobility in visually impaired subjects with retinitis pigmentosa. Three visits were scheduled over a 3-month period. Visit 1 (“screening”) included informed consent, eligibility screening, and visual assessment. Visit 2 comprised the mobility test. Visit 3 (“end of study”) included the same visual examinations as visit 1.

Visual assessment: Binocular distance VA was measured as the logarithm of minimum resolution angle (logMAR) using the ETDRS chart with usual correction. Letter CS was measured in logCS using the Pelli-Robson chart. This test reaches a maximum limit of 1.95. Binocular kinetic VF was measured in degrees with III4e Goldmann test using Octopus 900, Haag-Streit Diagnostics, Bern, Switzerland. Angular velocity was 4 degrees/s for each isopter and reaction time measured. Area and horizontal and vertical diameters were collected. As there was no significant difference between these 3 types of measures, horizontal VF was used for data processing and all VF references in this article. Dark adaptation (DA) was measured with Metrovision MonPackOne, Perenchies, France, in binocular vision: measurements started with a light adaptation phase (300 cd/m^2) lasting 5 minutes, followed by a DA phase lasting 20 minutes to determine visual sensitivity recovery.

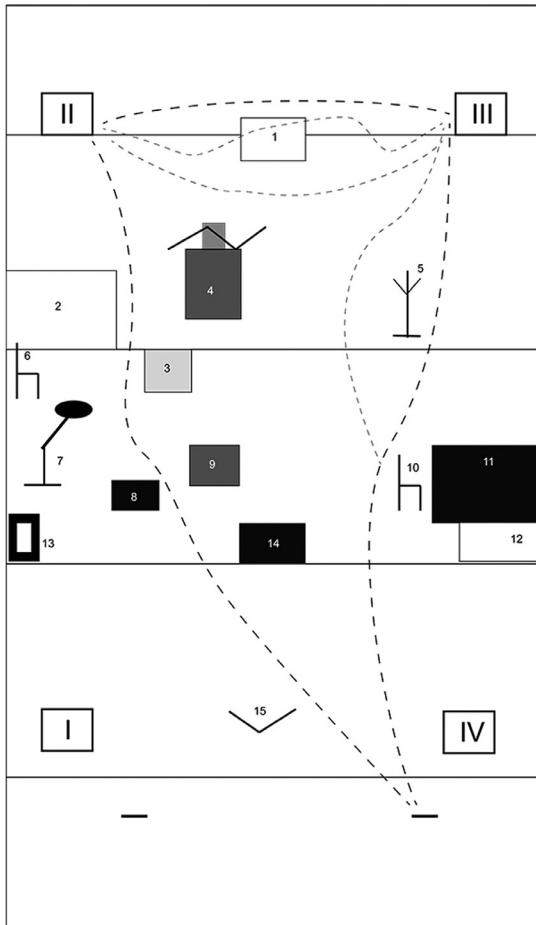
Study population and visual tests are summarized in Table 1.

Mobility assessment: Mobility was tested in 3 light settings: one at high illumination level (235 lux) and two at

low illumination levels (1 and 2 lux) (Figure 7). Four indoor courses (A, B, C, and D) comprising the same obstacles and length conditions were designed within the Streetlab artificial street platform (Figure 1). A 235 lux value was selected as corresponding to an optimal level of lighting required for movement in a corridor or stairs (between 100 and 300 lux) (standard: NF EN 12464-1), while 1 and 2 lux were chosen to mimic situations of darkness. For all light settings, the color temperature used was 4,350 K, which corresponded to a neutral value (NF X 35-103). The adaptation time to low illumination was 10 minutes because there were periods of transition but also periods of re-adaptation. The adaptation time to low illumination—10 minutes—was chosen based on a literature review.^{21,22}

All subjects were tested with the same obstacle settings. They were instructed to walk at a comfortable pace, without touching any obstacle. The task was conducted under 5 lighting conditions: after adaptation of 5 minutes at 235 lux and 10 minutes at 2 lux and 1 lux, and during the transition phase, with the test starting when the light changed from 235 lux to 1 or 2 lux. A set of 9 LED panels fixed to the ceiling provided the source of light (Figure 7). The subjects underwent 4 random courses (A, B, C, and D) under each lighting condition.

A Vicon motion capture system was used for part of the mobility performance measures (Figures 8 and 9) and recorded: time to complete a course; length (in meters); preferred walking speed (PWS) (time taken to walk 6 meters in a straight line with no obstacles); percentage of preferred walking speed (PPWS); walking initiation time (WIT) (time elapsed between the go signal [the instructor removes the screen hiding the scene from the test subject] and the first heel detachment from the ground); the number of segments of the trajectory (the trajectory of the torso center was modeled with the simplified Ramer-Douglas-Peucker algorithm [epsilon value 20 cm] to identify changes in direction using inflexion points, eg, a fracture corresponds to a turn). A fracture was rated as significant for angles greater than 39.6 degrees to filter out noise; for example, small curves related to calculation errors or noise in the Vicon signal (Figure 3); number of



- I / II / III / IV. Big white polystyrene blocks
- 1. white box
- 2. wood table
- 3. mannequin
- 4. big grey polystyrene block + plant + screen

- 5. coat rack
- 6. chair
- 7. floor lamp
- 8. black box
- 9. little grey polystyrene block
- 10. chair

- 11. black table
- 12. crate
- 13. little box + piece of paper
- 14. black coffee table
- 15. screen

----- Optimal path (expected trajectory)

----- Other correct options

FIGURE 7. Example of a course configuration (course A). The platform was converted into an open space with office equipment (eg, tables, boxes, chairs, coat rack, lamps, plants) spread around the room. The course was designed as a triangle with a large white polystyrene block (height: 55 cm; length: 35 cm; width: 30 cm) at each angle, and the same starting and arrival points. To vary the difficulty, 15 obstacles of different sizes and contrast (high and low) were set on the course. Eleven had a fixed location and 4 (obstacles 1, 5, 8, and 9) changed location according to the course (A, B, C, and D), to avoid an adjustment bias. The ceiling of the platform is composed of 9 LED panels that produce a homogeneous atmosphere at any point of the space and according to the 3 selected light settings.

collisions, defined as any part of the body making contact with an obstacle; and trajectory analyses were extracted from the videotape by a mobility instructor.

Second case study: Assessing mobility in subjects treated with Luxturna®. Four visits of visual assessments and mobility tests were scheduled over a 6-month period: before surgery

(visit 1 as baseline), 1 month after surgery (visit 2), 3 months after surgery (visit 3), and 6 months after surgery (visit 4).

Visual assessment: Best-corrected VA for each eye was measured as the logarithm of minimum resolution angle (logMAR) using the ETDRS chart at 4 meters and if the patient read less than 20 letters, the test was done at 1 me-

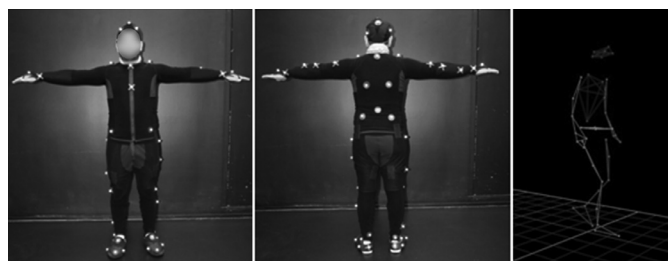


FIGURE 8. Vicon motion capture system description. The participants were equipped with a fitted velcro jumpsuit incorporating reflective markers on anatomical points based on the Plug-In-Gait (PIG) model. The latter reflected infrared emitted by Vicon cameras (T40), to collect walking parameters and head movements (not detailed).

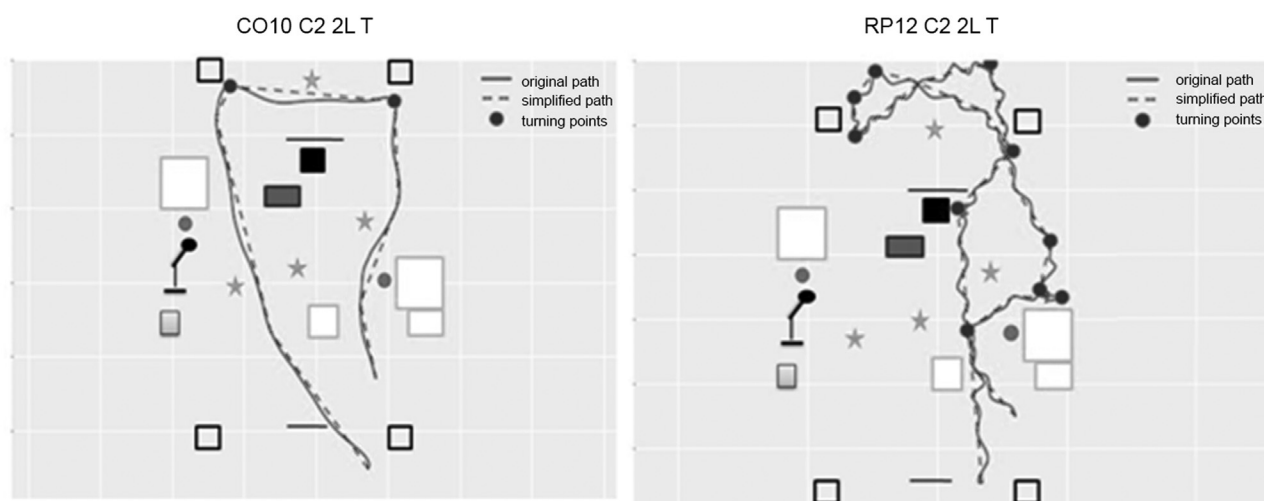


FIGURE 9. Examples of trajectory segmentation.

ter. Semi-kinetic VF for each eye was measured in degrees using the Octopus 900 (V4, III4e, I4e stimuli) except for children, for whom kinetic perimetry was performed using the Goldmann perimeter in manual mode (V4e, VI1e, VIIe, III1e stimuli). Full-field sensitivity threshold (FST) testing was performed to approach rod sensitivity across the retina independently of fixation²³ in subjects with RPE65-related LCA. OCT of the posterior pole was also performed.

Mobility assessment: Eight courses measuring approximately 22 m were designed to evaluate the evolution of mobility following the Luxturna[®] treatment. Like the first study, the visits took place in the Streetlab artificial street.

The courses differed by the location of 9 obstacles with different contrast and size (i.e., hose, bin, plants, public work sign, letterbox, tarpaulin, stepladder, flag [folded and unfolded], and white box; Figure 10) but were equivalent in difficulty. The 5 adults tested all 8 courses while the 3 children tested only 4 because the task had to be eased. Courses were presented randomly.

The patients were instructed to walk without touching any obstacle.

The task was conducted under 4 lighting conditions: after a 20-minute adaptation at 2 lux, after a 5-minute

adaptation at 7.5 lux, after a 5-minute adaptation at 50 lux, and after a 5-minute adaptation at 500 lux. Adult subjects took 2 courses each per lighting condition: one at a fast speed and one at a comfortable speed. The children took only one course at fast speed in each lighting condition. Figure 11 illustrates the experimental conditions.

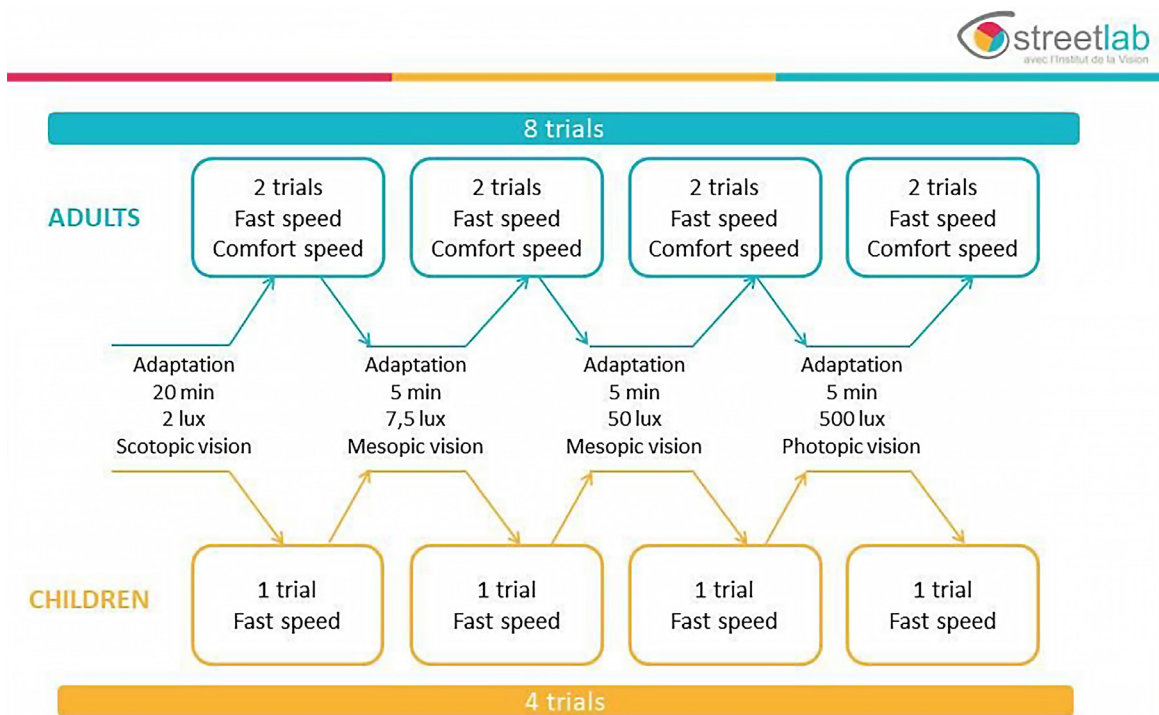
To measure changes in mobility performance, several variables were recorded: time to complete a course; PWS (i.e., time taken to walk 4 meters in a straight line with no obstacles); PPWS, calculated by dividing the average speed during the course by the PWS at fast speed 100; WIT (i.e., time elapsed between the go signal [the instructor removes the screen hiding the scene from the test subject] and the first heel detachment from the ground); the number of collisions, defined as any part of the body making contact with an obstacle; and trajectory analyses, extracted from the videotape by a mobility instructor.

Statistical analysis

First case study: Assessing mobility in visually impaired subjects with retinitis pigmentosa. The following data were collected: BCVA (logMAR), contrast sensitivity (logCS), VF area



FIGURE 10. Example of a mobility course presented to RPE65-related Leber congenital amaurosis subjects treated with Luxturna®.



For children : - Adaptation of instructions following the first visit of the subject 01.
- With 8 trials, the visit is too long.

FIGURE 11. Experimental conditions for Streetlab mobility test undertaken by RPE65-related Leber congenital amaurosis patients treated with Luxturna®.

(degree square), DA threshold (dB) at 1 and 10 minutes, mobility measures (PWS, PPWS, WIT), and number of collisions. Nonparametric tests were applied, as these variables do not fulfill a normality assumption. Repeated measurement analysis methods were not applicable, as base assumptions were not met.

Kruskal-Wallis tests served to compare mobility performances between the 5 light levels in each group and Mann-Whitney tests to compare visual parameters and mobility performance between both groups at each light level.

Correlations between visual data and mobility measures were investigated with Spearman correlation tests, both

TABLE 2. Comparison of Variables Between Retinitis Pigmentosa and Control Subjects

Variables	RP Group	Control Group	Mann-Whitney Test
VA	0.63 [0.30]	1.00 [0.00]	$P < .001^{***}$
MS	14.65 [10.55]	28.40 [2.45]	$P < .001^{***}$
CS	27.00 [9.00]	30.20 [1.50]	$P = .003^{**}$
OCT_Ep_0-1	253.00 [62.75]	264.00 [27.50]	$P = .058$
OCT_Ep_1-3	276.38 [48.56]	346.00 [24.50]	$P < .001^{***}$
OCT_Ep_3-6	233.13 [32.88]	304.50 [13.00]	$P < .001^{***}$
OCT_Volg	6.75 [1.05]	8.85 [0.41]	$P < .001^{***}$

RP = retinitis pigmentosa.
 $*P < .05$; $**P < .01$; $***P < .001$.

simple and multiple linear regressions. Data were analyzed using XLSTAT 2019.1 (Addinsoft, New York, New York, USA).

Second case study: Assessing mobility in subjects treated with Luxturna®. The results reported in this article are those of 2 patients: a child and an adult. Regarding the two case studies, only descriptive statistics were performed with Excel.

The following data were collected and analyzed: monocular VA (logMAR), VF area (degree square), FST (dB), OCT (retinal thickness in μm), and mobility measures (PPWS and number of collisions).

RESULTS

• **STUDIES OF MARKERS OF RETINITIS PIGMENTOSA WITH CONVENTIONAL CLINICAL IMAGING:** The mean age of the RP group (42.2 ± 14.6 years) was similar to the mean age of the control group (41.7 ± 14.0 years). The age and sex of the patients and controls were not statistically significantly different. The percentage sexes were 50.6% male and 49.4% female for RP and 26.7% male and 73.3% female for the control group.

All the measurable variables in the control group were significantly higher than those of the RP group, except for the retinal thickness of the 1 mm circle around the fovea (OCT_Ep_0-1) (Table 2).

In a first step, the correlation between the variables was carried out, as well as the determination of the severity criteria for each variable using decision trees. The correlation matrix between all the data is shown in Table 3.

Strong correlations exist between the functional criteria (VA, MS, and CS). VA is not strongly correlated to any structural variable. Correlation coefficients of 0.31-0.5 were found between VA and the vertical and horizontal internal diameters of the hyper-autofluorescence ring (FAF_GAH, FAF_GAV) and retinal thickness variables (OCT_EZh, OCT_ELMh, OCT_EZv et OCT_Ep_0-1).

MS is strongly correlated with the dimensions of the ring of increased FAF (GAH and GAV) and with OCT measures (preserved ellipsoid zone and external limiting membrane lengths [EZh, EZv, ELMh, ELMv, OCT_Ep_0-1, and OCT_Ep_1-3]). MS is correlated with the surface of the retina delimited by the ring of increased FAF (FAF_ACI), with a Pearson correlation coefficient $r = 0.42$. Central MS CS is strongly correlated with the other functional variables and with some OCT variables (EZh, EZv, ELMh, and ELMv), and to a lesser extent with the thickness variables (OCT_Ep_0-1, OCT_Ep_1-3, OCT_Ep_3-6, and OCT_Volg). Correlation of CS with FAF variables (FAF_GAH and GAV) is also lower ($r = 0.31$).

The dimensions of the ring of increased FAF (HAFh and HAFv) are not strongly correlated with the other FAF parameters.

For OCT data, we observe an important link between ellipsoid zone and external limiting membrane lengths. The foveal thickness (Ep_0-1) is significantly correlated only with ellipsoid zone parameters, and the parafoveal thickness (Ep_1-3) moderately correlated to external limiting membrane lengths and to the macular volume ($r = 0.45$, $r = 0.42$, and $r = 0.38$, respectively).

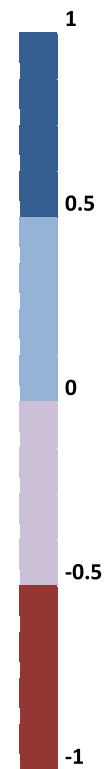
Tables 4–7 summarize the analysis of the discrimination values of the functional variables (VA and MS) for each structural variable.

Strong correlations are shown between all the functional variables and between all the structural variables of each modality. The mean MS is the most correlated variable to structural criteria and its discrimination value is higher than the VA variable. In a second step, we compared variables in 3 groups of patients according to the VA level (Table 7).

A post hoc Bonferroni test was used to compare the groups by pairs when the variance analysis (ANOVA) showed a significant difference (Table 8). The majority of the significant differences regarding the structural variables are observed between the most severe and the less severe groups ($VA \leq 0.3$ group and $VA > 0.7$ group). There were fewer differences between the most severe and intermediate groups ($0.3 < VA$ and $0.3 < VA \leq 0.7$) and between the intermediate and less severe groups ($0.3 < VA \leq 0.7$ and $VA > 0.7$).

TABLE 3. Correlation Matrix Between All the Data

	VA	MS	CS	FAF_ACI	FAF_Area HAF	FAF_GAH	FAF_HAFh	FAF_GAV	FAF_HAFv	OCT_EZh	OCT_ELMh	OCT_EZv	OCT_ELMv	OCT_vol1	OCT_vol3	OCT_vol6	OCT_volg
VA	1	0.61	0.69	0.21	0.04	0.41	-0.25	0.36	-0.21	0.42	0.32	0.37	0.28	0.49	0.3	-0.07	0.15
MS	0.61	1	0.74	0.42	0.19	0.65	-0.19	0.58	-0.11	0.65	0.55	0.6	0.5	0.57	0.52	0.19	0.25
CS	0.69	0.74	1	0.17	0	0.44	-0.31	0.36	-0.28	0.43	0.31	0.38	0.27	0.63	0.38	0.02	0.16
FAF_ACI	0.21	0.42	0.17	1	0.66	0.72	0.04	0.9	0.23	0.74	0.69	0.87	0.79	0.31	0.48	0.33	0.33
FAF_Area HAF	0.04	0.19	0	0.66	1	0.65	0.57	0.7	0.78	0.65	0.77	0.7	0.84	0.15	0.33	0.22	0.18
FAF_GAH	0.41	0.65	0.44	0.72	0.65	1	0.03	0.91	0.21	0.99	0.94	0.92	0.89	0.56	0.67	0.27	0.35
FAF_HAFh	-0.25	-0.19	-0.31	0.04	0.57	0.03	1	0.02	0.82	0.05	0.3	0.04	0.27	-0.21	-0.02	0.05	-0.01
FAF_GAV	0.36	0.58	0.36	0.9	0.7	0.91	0.02	1	0.24	0.91	0.86	0.99	0.93	0.49	0.59	0.28	0.34
FAF_HAFv	-0.21	-0.11	-0.28	0.23	0.78	0.21	0.82	0.24	1	0.23	0.45	0.25	0.51	-0.12	0.06	0.09	0
OCT_EZh	0.42	0.65	0.43	0.74	0.65	0.99	0.05	0.91	0.23	1	0.94	0.93	0.88	0.56	0.67	0.29	0.37
OCT_ELMh	0.32	0.55	0.31	0.69	0.77	0.94	0.3	0.86	0.45	0.94	1	0.88	0.92	0.45	0.59	0.26	0.31
OCT_EZv	0.37	0.6	0.38	0.87	0.7	0.92	0.04	0.99	0.25	0.93	0.88	1	0.94	0.51	0.6	0.28	0.34
OCT_ELMv	0.28	0.5	0.27	0.79	0.84	0.89	0.27	0.93	0.51	0.88	0.92	0.94	1	0.42	0.55	0.25	0.28
OCT_vol1	0.49	0.57	0.63	0.31	0.15	0.56	-0.21	0.49	-0.12	0.56	0.45	0.51	0.42	1	0.7	0.21	0.38
OCT_vol3	0.3	0.52	0.38	0.48	0.33	0.67	-0.02	0.59	0.06	0.67	0.59	0.6	0.55	0.7	1	0.65	0.66
OCT_vol6	-0.07	0.19	0.02	0.33	0.22	0.27	0.05	0.28	0.09	0.29	0.26	0.28	0.25	0.21	0.65	1	0.7
OCT_volg	0.15	0.25	0.16	0.33	0.18	0.35	-0.01	0.34	0	0.37	0.31	0.34	0.28	0.38	0.66	0.7	1



Significant correlations are dark blue ($r > 0.5$).

TABLE 4. Correlations Between Visual Acuity, Macular Sensitivity, and Fundus Autofluorescence Parameters

FAF-ACI	VA	FAF-ACI	MS	FAF-areaHAF	VA	FAF-areaHAF	MS
ACI≤0.03 (n = 18)	0.25 [0.12]	ACI≤0.21 (n = 28)	5.45 [4.83]	<i>No discrimination in relation to VA</i>		areaHAF≤1.12 (n = 29)	6.40 [6.50]
0.03<ACI≤0.28 (n = 11)	0.50 [0.16]	0.21<ACI≤1.07 (n = 34)	10.85 [3.53]			areaHAF>1.12 (n = 143)	16.0 [9.20]
ACI>0.28 (n = 143)	0.80 [0.50]	1.07<ACI≤4.45 (n = 76)	16.50 [7.23]			ACI>4.45 (n = 34)	
FAF-GAH	VA	FAF-GAH	MS	FAF-GAV	VA	FAF-GAV	MS
GAH≤227 (n = 18)	0.25 [0.12]	GAH≤595 (n = 28)	5.45 [4.83]	GAV≤195 (n = 18)	0.25 [0.12]	GAV≤589 (n = 30)	5.75 [5.00]
227<GAH≤595 (n = 10)	0.50 [0.19]	595<GAH≤1238 (n = 31)	10.60 [3.45]	195<GAH≤485 (n = 10)	0.50 [0.19]	589<GAV≤1095 (n = 29)	11.30 [4.90]
GAH>595 (n = 144)	0.80 [0.50]	1238<GAH≤2620 (n = 78)	16.25 [7.25]	GAV>485 (n = 144)	0.80 [0.50]	1095<GAV≤2052 (n = 75)	16.00 [7.38]
		GAH>2620 (n = 35)	22.80 [4.90]			GAV>2052 (n = 38)	21.30 [5.84]
FAF-HAFh	VA	FAF-HAFh	MS	FAF-HAFv	VA	FAF-HAFv	MS
HAFh≤378 (n = 62)	0.80 [0.38]	HAFh≤398 (n = 74)	16.25 [8.93]	HAFv≤447 (n = 134)	0.80 [0.38]	<i>No discrimination in relation to VA</i>	
HAFh>378 (n = 110)	0.63 [0.40]	HAFh>398 (n = 98)	12.75 [10.48]	HAFv>447 (n = 38)	0.50 [0.42]		

FAF = fundus autofluorescence; MS = macular sensitivity; VA = visual acuity.

TABLE 5. Correlations Between Visual Acuity and Macular Sensitivity and Ellipsoid Zone / External Limiting Membrane Lengths

OCT-EZh	VA	OCT-EZh	MS	OCT-EZv	VA	OCT-EZv	MS
EZh≤601 (n = 26)	0.32 [0.28]	EZh≤1,328 (n = 53)	7.70 [6.80]	EZv≤550 (n = 27)	0.32 [0.30]	EZv≤1097 (n = 55)	8.50 [6.85]
601<EZh≤4,224 (n = 138)	0.80 [0.30]	1,328<EZh≤2,687 (n = 84)	15.90 [7.45]	EZv>550 (n = 145)	0.80 [0.50]	1,097<EZv≤2,048 (n = 78)	15.75 [7.18]
EZh>4,224 (n = 8)	1.00 [0.20]	EZh>2,687 (n = 35)	22.10 [5.85]			EZv>2,048 (n = 39)	20.90 [5.58]
OCT-ELMh	VA	OCT-ELMh	MS	OCT-ELMv	VA	OCT-ELMv	MS
ELMh≤1,496 (n = 25)	0.32 [0.30]	ELMh≤1,656 (n = 34)	8.10 [6.23]	ELMv≤1,287 (n = 26)	0.32 [0.29]	ELMv≤1,663 (n = 49)	9.00 [6.40]
ELMh>1,496 (n = 147)	0.80 [0.45]	1,656<ELMh≤2,500 (n = 43)	13.50 [6.35]	ELMv>1,287 (n = 146)	0.80 [0.48]	1,663<ELMh≤2,292 (n = 55)	14.80 [7.45]
		2,500<ELMh≤3,617 (n = 58)	17.65 [7.81]			ELMv>2,292 (n = 68)	20.23 [8.43]
		ELMh>3,617 (n = 37)	22.10 [6.70]				

MS = macular sensitivity; VA = visual acuity.

When comparing the variables in the 3 groups according to the level of the mean MS, all the variables were significantly different except for the dimensions of the width of the ring of increased FAF (FAF_HAFh and FAF_HAFv) (Table 9). The comparison of the groups by pairs did not show a significant difference in surface of the ring of hyper-autofluorescence (FAF_Area-HAF). The variables FAF_ACI, OCT_Ep_1-3, OCT_Ep_3-6, and OCT_Volg are statistically significantly different between all groups, except between the most affected groups (MS ≤ 10 dB and 10 dB < MS ≤ 20 dB. All other criteria were

significantly different between all groups compared by pairs (Table 10).

We tested the interaction between the two functional factors (VA and retinal sensitivity, ANOVA test) and found a significant interaction only for the foveal sensitivity (CS) (P = .027).

When crossing the data of the VA groups and the MS groups, a Kruskal-Wallis test showed statistically significant differences of some variables between subgroups (Table 11). This step allowed us to show that the structural variables that reflect the level of functional alteration are the dimen-

TABLE 6. Correlations Between Visual Acuity and Macular Sensitivity and Retinal Thickness

OCT_Ep_0.1	VA	OCT_Ep_0.1	MS	OCT_Ep_1.3	VA	OCT_Ep_1.3	MS
EC≤182 (n = 21)	0.32 [0.25]	EC≤180 (n = 20)	5.05 [2.75]	Vol3≤311	0.63 [0.30]	Vol3≤250	9.60 [7.75]
182<EC≤222	0.50 [0.23]	180<EC≤223	10.70 [8.48]	(n = 136)	0.80 [0.37]	(n = 31)	14.55 [9.35]
(n = 26)	0.80 [0.38]	(n = 28)	14.50 [8.28]	Vol3>311		250<Vol3≤312	22.10 [4.63]
EC>222		223<EC≤269	20.10 [7.93]	(n = 36)		(n = 110)	
(n = 125)		(n = 64)				Vol3>312	
		EC>269 (n = 60)				(n = 31)	
OCT_Ep_3.6	VA	OCT_Ep_3.6	MS	OCT_Volg	VA	OCT_Volg	MS
<i>No discrimination in relation to MS</i>		Vol6≤255	14.05 [9.90]	Volg≤5.41	0.50 [0.37]	Volg≤7.1 (n = 123)	13.50 [8.90]
		(n = 134)	19.35 [12.18]	(n = 15)	0.80 [0.30]	Volg>7.1 (n = 49)	20.30 [9.40]
		Vol6>255		Volg>5.41			
		(n = 38)		(n = 157)			

MS = macular sensitivity; VA = visual acuity.

TABLE 7. Comparison of Variables Between Groups Divided According to Visual Acuity

Variables	VA ≤ 0.3 (n = 26)	0.3 < VA ≤ 0.7 (n = 64)	VA > 0.7 (n = 82)	ANOVA
VA	0.22 ± 0.08	0.53 ± 0.08	0.91 ± 0.13	<i>P</i> < .001***
MS	8.63 ± 5.51	12.30 ± 6.32	18.20 ± 5.74	<i>P</i> < .001***
CS	14.90 ± 7.60	24.00 ± 6.43	29.30 ± 3.96	<i>P</i> < .001***
FAF_ACI	1.41 ± 2.78	2.77 ± 4.24	5.30 ± 9.52	<i>P</i> = .014*
FAF_area-HAF	2.47 ± 3.72	3.49 ± 5.16	3.37 ± 3.36	<i>P</i> = .554
FAF_GAH	865.2 ± 1,236.8	1,634.5 ± 1,082.5	2,316.9 ± 1,213.9	<i>P</i> < .001***
FAF-HAFh	604.1 ± 381.4	495.6 ± 241.9	424.0 ± 170.7	<i>P</i> = .0035**
FAF-GAV	699.9 ± 1,028.5	1,405.7 ± 1,006.5	2,010.0 ± 1,381.6	<i>P</i> < .001***
FAF_HAFv	478.9 ± 264.1	421.2 ± 292.6	355.0 ± 140.5	<i>P</i> = .037*
OCT-EZh	918.9 ± 1,196.5	1,713.0 ± 1,106.1	2,394.9 ± 1,237.6	<i>P</i> < .001***
OCT_ELMh	1,970.8 ± 1,451.0	2,647.7 ± 1,288.9	3,198.4 ± 1,288.4	<i>P</i> < .001***
OCT_EZv	773.5 ± 1,018.8	1,453.4 ± 984.1	2,019.4 ± 1,233.9	<i>P</i> < .001***
OCT_ELMv	1,652.9 ± 1,199.7	2,270.1 ± 1,266.7	2,705.0 ± 1,232.5	<i>P</i> < .001***
OCT_Ep_0-1	203.3 ± 53.2	238.7 ± 46.9	272.1 ± 37.0	<i>P</i> < .001***
OCT_Ep_1-3	266.6 ± 39.0	277.9 ± 33.2	290.8 ± 33.8	<i>P</i> = .001**
OCT_Ep_3-6	239.1 ± 32.4	240.1 ± 29.5	233.8 ± 27.1	<i>P</i> = .369
OCT_Volg	6.44 ± 1.08	6.73 ± 1.02	6.79 ± 0.93	<i>P</i> = .271

VA = visual acuity.

P* < .05; *P* < .01; ****P* < .001.

sions of the ring of hyper-autofluorescence (FAF_GAH and FAF_GAV), the lengths of the ellipsoid zone and external limiting membrane (OCT_EZh, OCT_EZv, OCT_ELMh, and OCT_ELMv), and the foveal thickness (OCT_Ep_0-1).

In addition, by crossing the groups according to VA and to MS, we learned that at early stage of disease, when the VA is preserved (VA > 0.3), the variable MS most reliably reflects the impact of structural changes. At late and advanced stages, when MS is inferior to 10 dB, VA could be correlated with structural changes.

• **HIGH-RESOLUTION ADAPTIVE OPTICS RETINAL IMAGING:** Images were reviewed by 3 experts in AO imaging (authors K.G., M.P., J.A.S.) and a consensual interpretation

was obtained. Only cases with clear evidence of a photoreceptor mosaic in the central 2 degrees were analyzed. We excluded cases showing evidence of foveal cysts by OCT or any media opacity. Most patients had an oval-shaped patch of photoreceptors covering between 2 and 6 degrees from the fovea (that is, spanning 4-12 degrees overall) corresponding to moderate-to-severe stages (Figure 12).

A variety of phenotypes were observed: paradoxical visibility of foveal cones, heterogeneous brightness of cones, dim mosaic, inner segment-like mosaic, RPE-like mosaic. Additionally, we identified two factors that added variability to the photoreceptor imaging: directional illumination by varying the orientation of the incident light (Stiles-Crawford effect) and the amount of side illumination (gaze-dependent imaging).

TABLE 8. Comparison of Variables Between the Groups by Pairs

Variables	VA ≤ 0.3 – 0.3 < AV ≤ 0.7	0.3 < VA ≤ 0.7 – VA > 0.7	VA ≤ 0.3 – VA > 0.7
VA	S*	S*	S*
MS	S*	S*	S*
CS	S*	S*	S*
FAF_ACI	NS	NS	S*
FAF_Area-HAF	ANOVA not significant		
FAF_GAH	S*	S*	S*
FAF_HAFh	NS	NS	S*
FAF_GAV	S*	S*	S*
FAF_HAFv	NS	NS	NS
OCT_EZh	S*	S*	S*
OCT_ELMh	S*	S*	S*
OCT_EZv	S*	S*	S*
OCT_ELMv	NS	NS	S*
OCT_Ep_0-1	S*	S*	S*
OCT_Ep_1-3	NS	S*	S*
OCT_Ep_3-6	ANOVA not significant		
OCT_Volg	ANOVA not significant		

VA = visual acuity.
S*: $P < .05$; NS: $P \geq .05$.

TABLE 9. Comparison of Variables Between Groups Divided According to the Level of Macular Sensitivity

Variables	MS ≤ 10 dB (n = 49)	10 dB < MS ≤ 20 dB (n = 78)	MS > 20 dB (n = 45)	Test ANOVA
VA	0.22 ± 0.08	0.53 ± 0.08	0.91 ± 0.13	$P < .001^{***}$
MS	8.63 ± 5.51	12.30 ± 6.32	18.20 ± 5.74	$P < .001^{***}$
CS	14.90 ± 7.60	24.00 ± 6.43	29.30 ± 3.96	$P < .001^{***}$
FAF_ACI	1.41 ± 2.78	2.77 ± 4.24	5.30 ± 9.52	$P < .001^{***}$
FAF_Area-HAF	2.47 ± 3.72	3.49 ± 5.16	3.37 ± 3.36	$P = .046^*$
FAF_GAH	865.2 ± 1,236.8	1,634.5 ± 1,082.5	2,316.9 ± 1,213.9	$P < .001^{***}$
FAF_HAFh	604.1 ± 381.4	495.6 ± 241.9	424.0 ± 170.7	$P = .400$
FAF_GAV	699.9 ± 1,028.5	1,405.7 ± 1,006.5	2,010.0 ± 1,381.6	$P < .001^{***}$
FAF_HAFv	478.9 ± 264.1	421.2 ± 292.6	355.0 ± 140.5	$P = .872$
OCT_ZEh	918.9 ± 1,196.5	1,713.0 ± 1,106.1	2,394.9 ± 1,237.6	$P < .001^{***}$
OCT_ELMh	1,970.8 ± 1,451.0	2,647.7 ± 1,288.9	3,198.4 ± 1,288.4	$P < .001^{***}$
OCT_EZv	773.5 ± 1,018.8	1,453.4 ± 984.1	2,019.4 ± 1,233.9	$P < .001^{***}$
OCT_ELMv	1,652.9 ± 1,199.7	2,270.1 ± 1,266.7	2,705.0 ± 1,232.5	$P < .001^{***}$
OCT_Ep_0-1	203.3 ± 53.2	238.7 ± 46.9	272.1 ± 37.0	$P < .001^{***}$
OCT_Ep_1-3	266.6 ± 39.0	277.9 ± 33.2	290.8 ± 33.8	$P < .001^{***}$
OCT_Ep_3-6	239.1 ± 32.4	240.1 ± 29.5	233.8 ± 27.1	$P = .0016^{**}$
OCT_Volg	6.44 ± 1.08	6.73 ± 1.02	6.79 ± 0.93	$P < .001^{***}$

MS = macular sensitivity.
* $P < .05$; ** $P < .01$; *** $P < .001$.

Paradoxical visibility of cones in the fovea

With the rtx1 camera, the normal fovea appears as a uniformly grayish area. An example of paradoxical visibility of the cones in the fovea is shown in [Figure 13](#). These cones appear in most cases as isolated spots dispersed within a

uniform foveal background. As the nominal resolution of the rtx1 camera is 2 μm, the fact that some cones are visible in the center of the fovea suggests that they are enlarged, and hence that there is a loss of central cones; the enlargement of adjacent photoreceptors following the loss of some

TABLE 10. Comparison of the Variables of the Sensitivity Groups Two by Two

Variables	MS ≤ 10 dB – 10 dB < MS ≤ 20 dB	10 dB < MS ≤ 20 dB – MS > 20 dB	MS ≤ 10 dB – MS > 20 dB
VA	S*	S*	S*
MS	S*	S*	S*
CS	S*	S*	S*
FAF_ACI	NS	S*	S*
FAF_Area-HAF	NS	NS	NS
FAF_GAH	S*	S*	S*
FAF_HAFh	ANOVA not significant		
FAF_GAV	S*	S*	S*
FAF_HAFv	ANOVA not significant		
OCT_EZh	S*	S*	S*
OCT_ELMh	S*	S*	S*
OCT_EZv	S*	S*	S*
OCT_ELMv	S*	S*	S*
OCT_Ep_0-1	S*	S*	S*
OCT_Ep_1-3	NS	S*	S*
OCT_Ep_3-6	NS	S*	S*
OCT_Volg	NS	S*	S*

MS = macular sensitivity.
S*: $P < .05$; NS: $P \geq .05$.

TABLE 11. Variables Between Subgroups by Kruskal-Wallis Test; Significativity Analysis Between the Subgroups When Crossing the Visual Acuity and Macular Sensitivity Groups

Variables	VA ≤ 0.3 (n = 26)	0.3 < VA ≤ 0.7 (n = 64)	VA > 0.7 (n = 82)	Variables With a Significant Kruskal-Wallis Test
MS ≤ 10 dB (n = 49)	n = 16	n = 23	n = 10	VA/MS/CS/FAF: ACI/ GAH/ GAV//OCT: EZh/ ELMh/ EZv/ ELMv/ Ep_0-1
10 dB < MS ≤ 20 dB (n = 78)	n = 10	n = 33	n = 35	VA/ CS/OCT_Ep_0-1
MS > 20 dB (n = 45)	n = 0	n = 8	n = 37	VA
Variables with a significant Kruskal-Wallis test	MS/CS/OCTvol1	VA/ MS/ CS/FAF: ACI/ Area-HAF/ GAH/ GAV//OCT: EZh/ ELMh/ EZv/ ELMv/ Ep_0-1/ Ep_1-3	VA/ MS/ CS/FAE: ACI/ Area-HAF/ GAH/ GAV//OCT: EZh/ ELMh/ EZv/ ELMv/ Ep_0-1/ Ep_1-3/ Ep_3-6 / Volg	

CS = contrast sensitivity; FAF = fundus autofluorescence; MS = macular sensitivity; OCT = optical coherence tomography; VA = visual acuity.

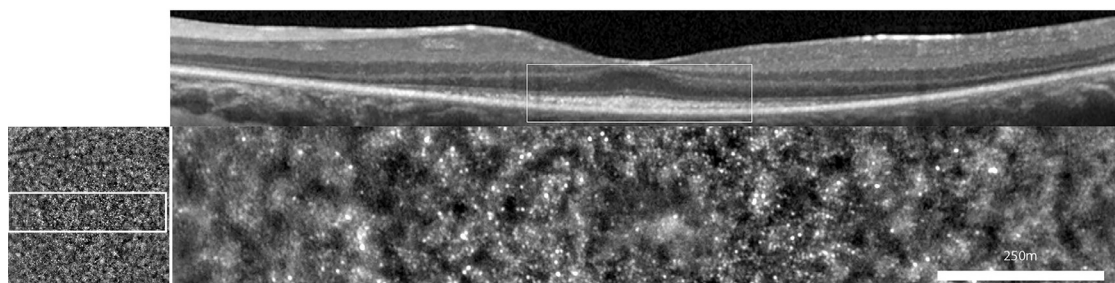


FIGURE 12. Central patch of cone mosaic seen by optical coherence tomography (Top) and by flood adaptive optics-enhanced ophthalmoscopy (Bottom). Female patient affected with simplex rod-cone dystrophy of unknown genotype, since the subject denied testing.

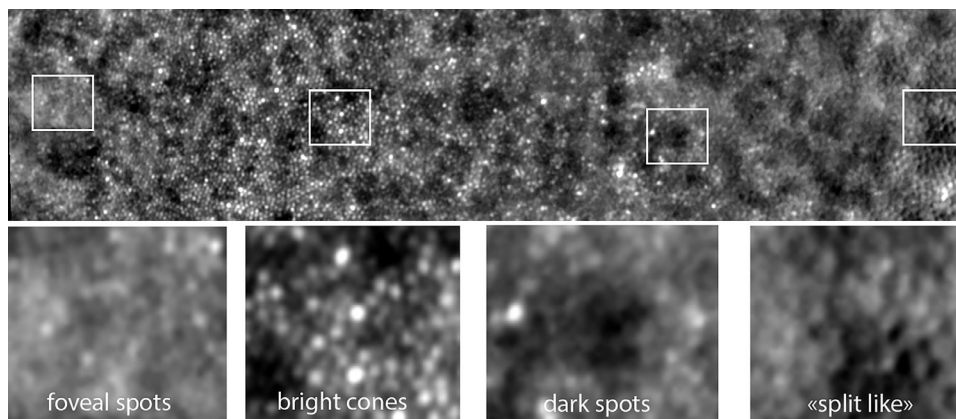


FIGURE 13. Illustration of different cone phenotypes.

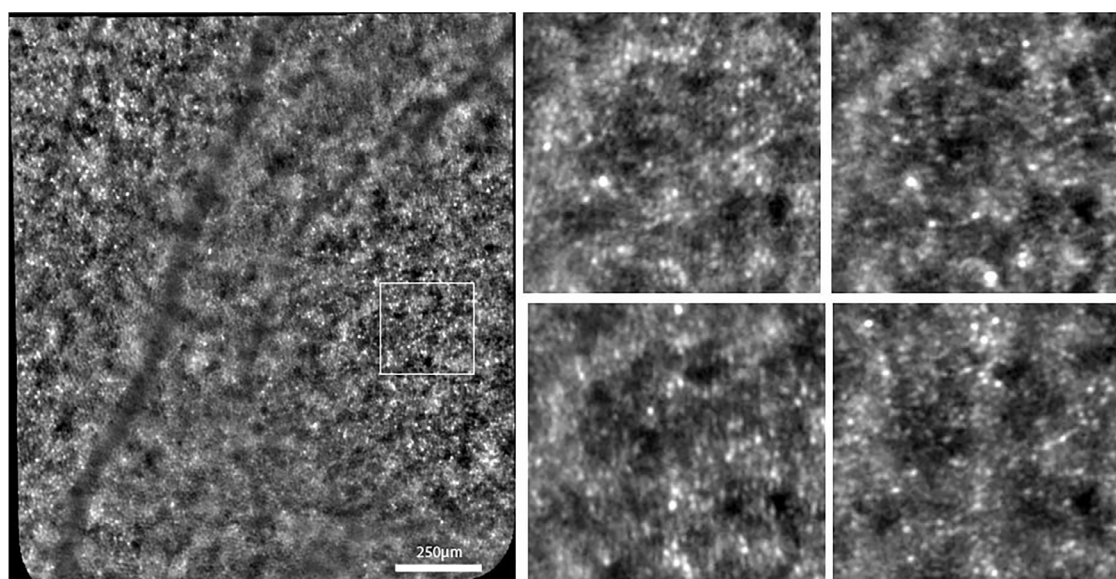


FIGURE 14. Illustration of the effect of directional imaging on the visualization of the cone mosaic. Left, reference (on-axis) image; Right, images of the area located in the square seen at 4 different off-axis light incidences. Note the variation in the appearance of the cone mosaic. Case of a 28-year-old man with rod-cone dystrophy associated with a likely pathogenic homozygous variant in *USH2A* (NM_206933.2; c.4628-2A>T).

of them is indeed a known property of photoreceptors.²⁴ However, the resolution refers solely to the separation between two light sources, and not to the brilliance of an individual spot. Hence, it is not yet certain if the visibility of isolated cones is an indication of loss of cones in the fovea or an increase in their brightness. Nevertheless, it is of interest to note that these paradoxically visible cones were observed only in the 3 most severely affected eyes.

“Brilliant cones”

An example of “brilliant cones” is shown in Figure 14. These highly reflective spots were visible within a normal-appearing mosaic. These brilliant cones are isolated from one another and also appear larger. They seem to be present in the most severely affected cases.

Dim mosaic

Split detection using scan-based systems has become a widely used procedure to analyze the cone mosaic.²⁵ It is assumed that the so-called split detection procedure detects the inner segments, hence being able to detect remnant cones (“dormant cones”) within areas showing disappearance of outer segments on OCT or reflectance imaging. Interestingly, with FIAO we identified a mosaic in the periphery of atrophic areas that was highly similar to that reported for split detection. The fact that it was only detected where outer segments had disappeared, yet at the same time showing persistence of the inner/outer segment limit on OCT scans, supports the hypothesis that the observed mosaic was indeed that of the inner segments.

RPE-like mosaic

It is assumed that the hyper-autofluorescent ring around the parafoveal area of preserved photoreceptors is due to the loss of outer segments, which increases the amount of excitation light accessing RPE cells and also the amount of re-emitted fluorescent light toward the camera. Accordingly, we observed that the RPE mosaic could be clearly distinguished in areas showing absent outer segments. This was also observed in a case of drug-induced toxicity to outer segments.²⁶ This demonstrates that RPE cells may maintain a seemingly normal distribution and shape for years despite the disappearance of detectable outer segments

Stiles-Crawford effect

Normal cone outer segments show a high degree of parallelism. Central photoreceptors usually point toward the center of the pupil, slightly nasally. However, the physical orientation of outer segments may not be always toward the observation axis, even in normal eyes, in particular in the periphery, which may generate the so-called “negative cone mosaic.”²⁷ The orientation of outer segments can theoretically be determined by the angle-response curve of individual cones, which is assumed to be a Gaussian curve defined by its height, the orientation, and the rho (ie, the width). Using the rtx1 camera, a simple way for screening for misaligned cones is to compare images taken at different light incidences, which requires a dilated pupil. Once processed and aligned, outer segments showing differing orientation can be detected by alternating between the two angled views. These misaligned cones can occur in patches such as during acute macular neuroretinopathy.²⁸ In the latter disease, it seems that adjacent outer segments maintain parallelism over relatively large areas (covering hundreds or thousands of cones).

A simple approach to quantify the degree of photoreceptor outer segment misalignment is to compare individual images to cumulative sum images. Indeed, a simple image processing can be done to additively select bright pixels, hence establishing a cumulative map of the outer segment density. The respective proportion of cones detected by simple vs cumulative maps gives a crude estimate of photoreceptor misalignment. In a population of RP patients, we determined that cumulative images enabled us to increase automated counts by 164% on average (range, 108%-246%). Comparatively, in an age-matched control population, the increase was 25% in corresponding areas (Azoulay and colleagues, unpublished data). This suggests that residual cones in RP patients show a greater degree of misalignment than controls. An alternative explanation, however, is that the rho of photoreceptors (ie, the angle of acceptance of photons of individual cones) is smaller in RP eyes, hence requiring a better alignment of the observation for them to be detected. Whatever the explanation, this shows that to have an accurate estimate of the density of outer segments, compensating for the Stiles-Crawford effect should be considered.

Gaze-dependent imaging

Gaze-dependent variability of AO images has been reported for drusen.²⁹ Here, we report for the first time that the photoreceptor mosaic may show significant variability between images taken over a different field of view. Indeed, in most cases of RP, it appears that cones are more visible if they are closer to the center of the field of view. This has a potentially important consequence; that is, cones located at the border of photoreceptor patches are less likely to be detected if the field of view is not centered on them. In other words, photoreceptor counts are probably more reliable in the center of the field of view.

Gaze-dependent variability is clearly different from directional illumination; indeed, two images taken at different fields of view do not show variation of vascular shadowing, which is typically observed when varying the illumination angle. An example of gaze-dependent variability of cone imaging is shown in [Figure 15](#).³⁰

A possible contributing factor for such variability is that the backscattered light is increased in RP, possibly because there are fewer outer segments to “filter” the light accessing and reflected back from the RPE and choroid. The absence of a pinhole in FIAO cameras results in the absence of filtering of these out-of-focus photons. Since it is likely that side-scattered light contributes to the uneven distribution of light in the images, this may contribute to lessen the contrast of eccentric photoreceptors.

• ASSESSING FUNCTIONAL VISION:

First case study: Assessing mobility in visually impaired subjects with retinitis pigmentosa

Visual field assessment in subjects with retinitis pigmentosa. Area and horizontal and vertical diameters were collected. As there was no significant difference between these 3 types of measures, horizontal VF was used for data processing and all VF references in this article.

Table 1 contains demographic data and clinical measures of visual function for both RP and CO subjects. Within the RP group, the visual function measures were all correlated (from $P = .0003$ to $P < .0001$), except DA 10' and VA ($P = .108$).

Mobility assessment in subjects with retinitis pigmentosa. As shown in [Figure 16](#), poorer results were observed in the RP group than in the control group for PWS, PPWS, WIT, and number of collisions for both low illumination ($P < .0001$) and high illumination ($P < .0001$, $P < .0001$, $P = .0001$, $P = .001$, respectively). The mean number of segments was higher in the RP group for low illumination ($P < .01$); no significant difference between the two groups was found at high illumination (235 lux).

Predicting mobility performance with objective visual parameters. Linear multiple regression analyses suggested that the studied mobility variables were not all explained by

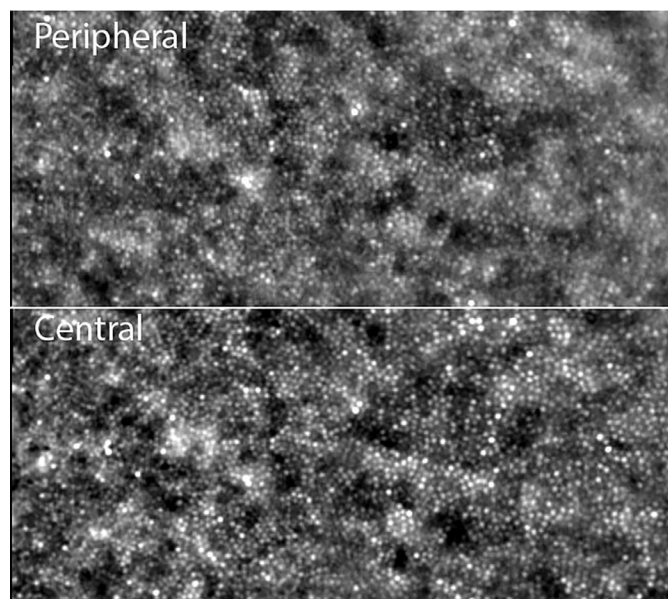


FIGURE 15. Adaptive optics–enhanced ophthalmoscopy images illustrating the effect of gaze positioning on cone imaging. Both images show the same retinal area; in the top image this area was located on the image margin, while in the bottom the same area was placed centrally. Note the better visualization of the cone mosaic when placed in the center of the field of view (that is, the bottom image). Case of a 33-year-old male patient with rod-cone dystrophy of unknown genetic defect after screening on a 254 targeted gene next-generation sequencing panel (Audo et al, ref. 30).

TABLE 12. Results of Linear Multiple Regression Analysis

	PWS	WIT	Number of Collisions	PPWS	Segments
235L A	Age+VF $P < .0001$ $R^2_{adj} = 0.70$	CS+VF $P = .001$ $R^2_{adj} = 0.57$	Age+VF $P = .037$ $R^2_{adj} = 0.29$	Age+VF $P = .033$ $R^2_{adj} = 0.30$	CS+VF $P < .0001$ $R^2_{adj} = 0.73$
2L A	Age+VF $P < .0001$ $R^2_{adj} = 0.73$	VA+VF $P = .024$ $R^2_{adj} = 0.33$	Age+CS $P = .001$ $R^2_{adj} = 0.58$	VA+DA $P = .021$ $R^2_{adj} = 0.44$	CS+VA $P = .001$ $R^2_{adj} = 0.56$
2L T	CS $P = .001$ $R^2_{adj} = 0.495$	Age+VF $P = .039$ $R^2_{adj} = 0.28$	Age+CS $P < .0001$ $R^2_{adj} = 0.72$	DA $P = .002$ $R^2_{adj} = 0.49$	Age+CS $P < .0001$ $R^2_{adj} = 0.74$
1L A	Age+VF $P < .0001$ $R^2_{adj} = 0.73$	Age+VF $P = .019$ $R^2_{adj} = 0.35$	CS+VF $P < .0001$ $R^2_{adj} = 0.8$	DA $P = .007$ $R^2_{adj} = 0.452$	CS $P < .0001$ $R^2_{adj} = 0.902$
1L T	Age+VF $P < .0001$ $R^2_{adj} = 0.62$	Age+VF $P = .011$ $R^2_{adj} = 0.4$	CS+VF $P = .0003$ $R^2_{adj} = 0.64$	Age+DA $P = .005$ $R^2_{adj} = 0.52$	Age+CS $P < .0001$ $R^2_{adj} = 0.865$

CS = contrast sensitivity; DA = dark adaptation; PPWS = percentage of preferred walking speed; PWS = preferred walking speed; VA = visual acuity; VF = visual field; WIT = walking initiation time.

the same visual parameter (Table 12). At 235 lux, VF was a predictor for all mobility performance models, associated with age or CS.

Under low illumination, VF was the most significant predictor of mobility performance variables related to time, PWS, and WIT, while CS best explained the number of collisions and segments. In our conditions, for most of the

time, each of them was combined with age. Neither VF nor CS was a significant predictor of PPWS. DA explained 44%-52% of the variance by itself or associated with VA or age.

Second case study: Assessing mobility in subjects treated with Luxturna®

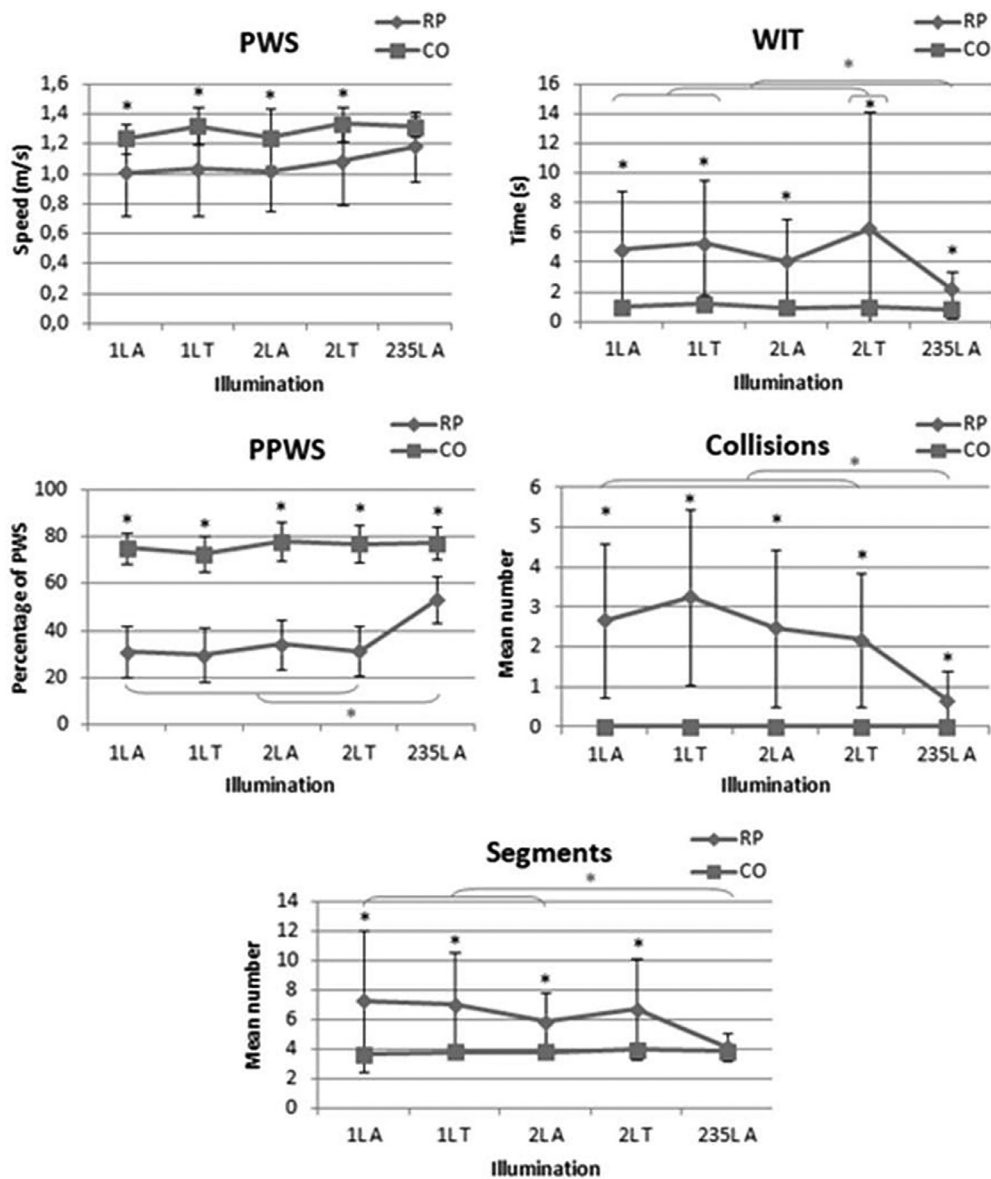


FIGURE 16. Mobility performance in retinitis pigmentosa (RP) and control (CO) groups under different lighting conditions. PPWS = percentage of preferred walking speed; PWS = preferred walking speed; WIT = walking initiation time.

Visual assessment in subjects treated with Luxturna®. Visual tests results are summarized in Table 13 (where the retinal thickness was determined by OCT). Subjectively both patients reported a significant improvement of their vision, particularly in dim light conditions.

VA did not change significantly after treatment, but a small increase was measured (a gain of 1-2 lines is observed in the young patient). Regarding VF, despite the variability of the test, we observed a notable improvement in the surfaces of isopters after treatment in both eyes in adult and young patients. Manual Goldmann kinetic perimetry was performed in the young patient, so we did not calculate the surfaces but observed a large extension of isopters. The surface the III4e isopter of the binocular visual central island had less than 20 degrees of diameter before treatment,

and enlarged to more than 140 degrees with a thin ring scotoma (Figure 17). As expected, mean white FST testing improved for both patients from -3 dB in average in the young patient and -5 dB in the adult patient to nearly -50 dB and -30 dB, respectively, after treatment.

Mobility assessment. PPWS results: The child PPWS increased with each visit in all lighting conditions. We observed a similar evolution of the adult PPWS in 2 and 7.5 lux, but its increase was less significant at 50 lux, although it was still much better 6 months after treatment than baseline before treatment (Figure 18). Moreover, in contrast to mesopic conditions where the PPWS increased with each visit, the adult PPWS was higher (72.3% vs

TABLE 13. Evolution of Visual Data According to Visits

		Right Eye				Left Eye			
		Visit 1	Visit 2	Visit 3	Visit 4	Visit 1	Visit 2	Visit 3	Visit 4
Visual field V4e (deg ²)	Child Manual								
	Adult Semi-kinetic	11,103	11,344	14,754	9,199	9,438	10,925	12,174	10,407
Visual field III4e (deg ²)	Child Manual								
	Adult Semi-kinetic	1,582	3,383	6,692	9,199	669	3,616	3,945	3,165
Visual acuity (logMAR)	Child	1.1	0.8	0.8	0.7	1.1	1.1	0.9	0.9
	Adult	0.8	0.9	1	1	0.9	0.9	1	1
FST (dB)	Child	-3.1	-41.6	-29.5	-47.2	-3	-47.5	-35.2	-73.6
	Adult	-5.5	-43.4	-37.9	-37.7	-4.8	-34.2	-30.1	-28.8
OCT (μm)	Child	214	217	212	210	201	195	198	200
	Adult	205	184	188	195	206	168	170	174

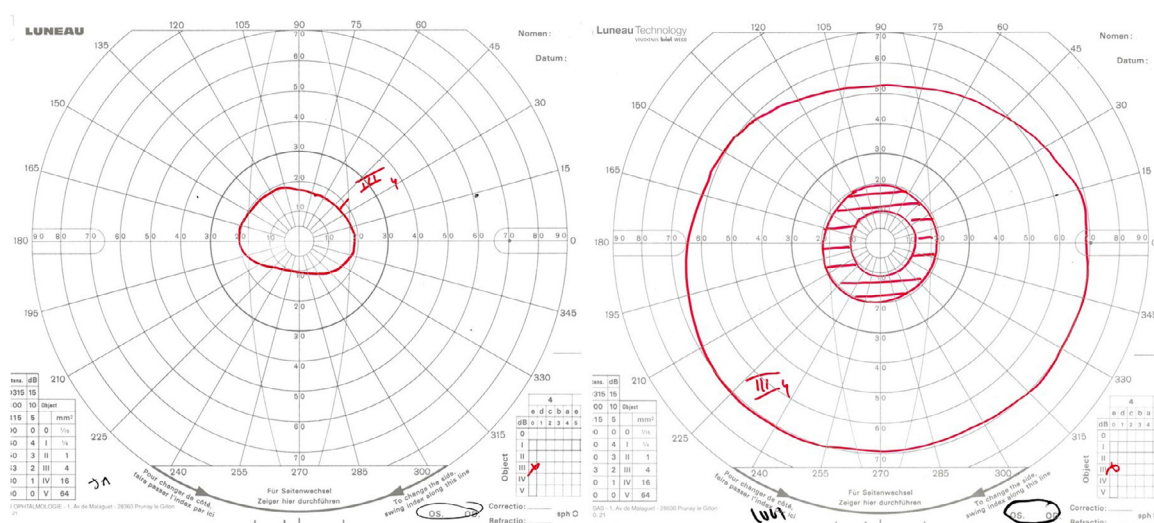


FIGURE 17. Manual Goldmann kinetic perimetry in the young patient. The surface the III4e isopter of the binocular visual central island had less than 20 degrees of diameter before treatment, and enlarged to more than 140 degrees with a thin ring scotoma.

20%-40%) from the first visit at 500 lux and tended to remain stable over time.

The graphs presented in Figure 19 show the relative variation for the PPWS according to the four visits. The most significant relative variation of the PPWS was observed at 2 lux between baseline (visit 1 before injection) and 6 months after injection (visit 4) for the child (gain of 240%) and for the adult (gain of 188%).

Collisions: In contrast to PPWS, which improved with each post-treatment visit (visit 2 to visit 4), the number of collisions improved significantly between visit 1 and visit 2 (Figures 20 and 21).

At 2 lux, the child hit 9 obstacles before treatment (visit 1). This number dropped to 2 at visit 2 (1 month after treatment) and then to 1 at visits 3 4. At 7.5, 50, and 500 lux, the only recorded collisions were observed at visit 1; after treatment, the child did not hit any obstacles at all.

A drop in the number of collisions before and after treatment was also observed in the adult subject, although it was

more progressive, especially at 2 lux. A few collisions were still recorded after treatment, especially at visit 2, until they also completely disappeared from visit 3 at 50 and 500 lux.

DISCUSSION

- **ADAPTING THE THERAPEUTIC STRATEGY TO THE STATUS OF THE RETINA REQUIRES AN ASSESSMENT OF THE DISEASE STAGE:** Disease staging represents an essential aspect of retinal evaluation. It is of critical importance for patient selection for clinical studies and choice of the most appropriate treatment for every individual patient, in addition to evaluation of the disease progression (expected pattern and outcome), and assessing treatment results among patients and patient groups.

More than 30 gene replacement trials are currently ongoing,³¹ some of them in the late phase of clinical research.

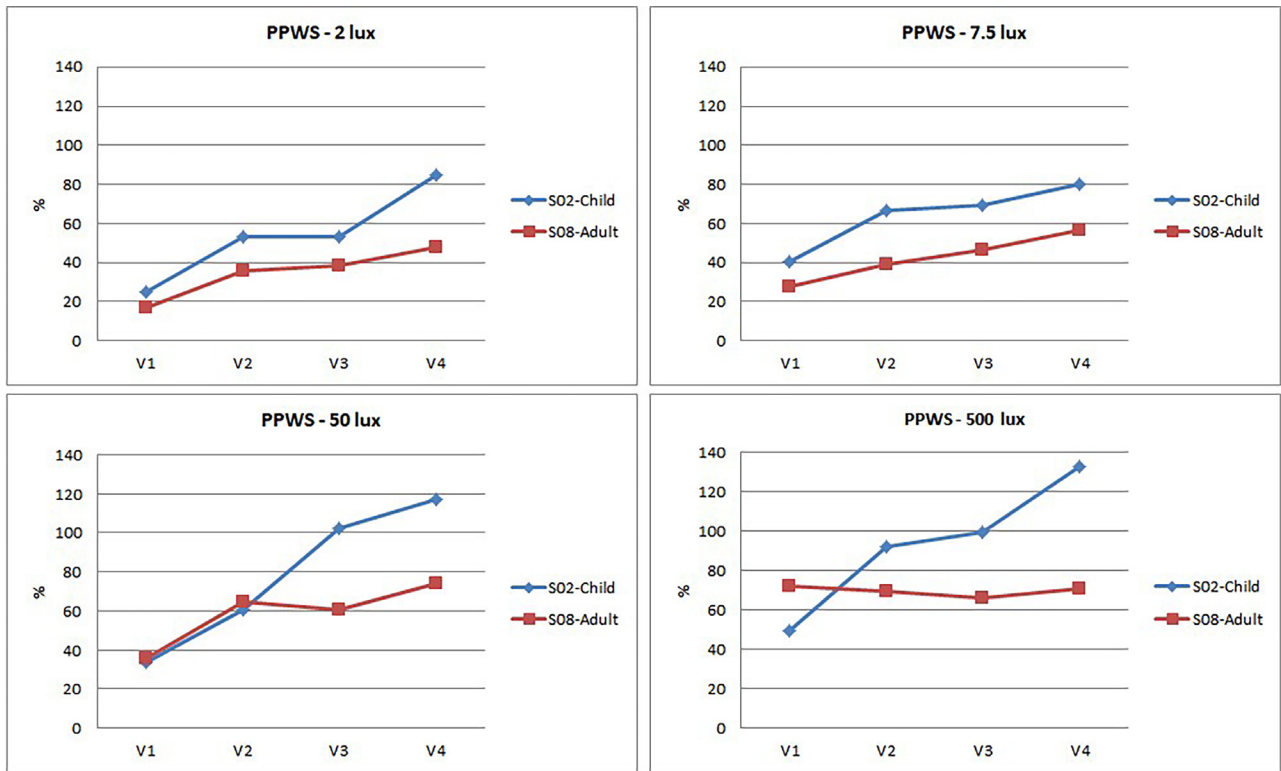


FIGURE 18. Evolution of the percentage of preferred walking speed (PPWS) according to lighting conditions and visits. V = visit.

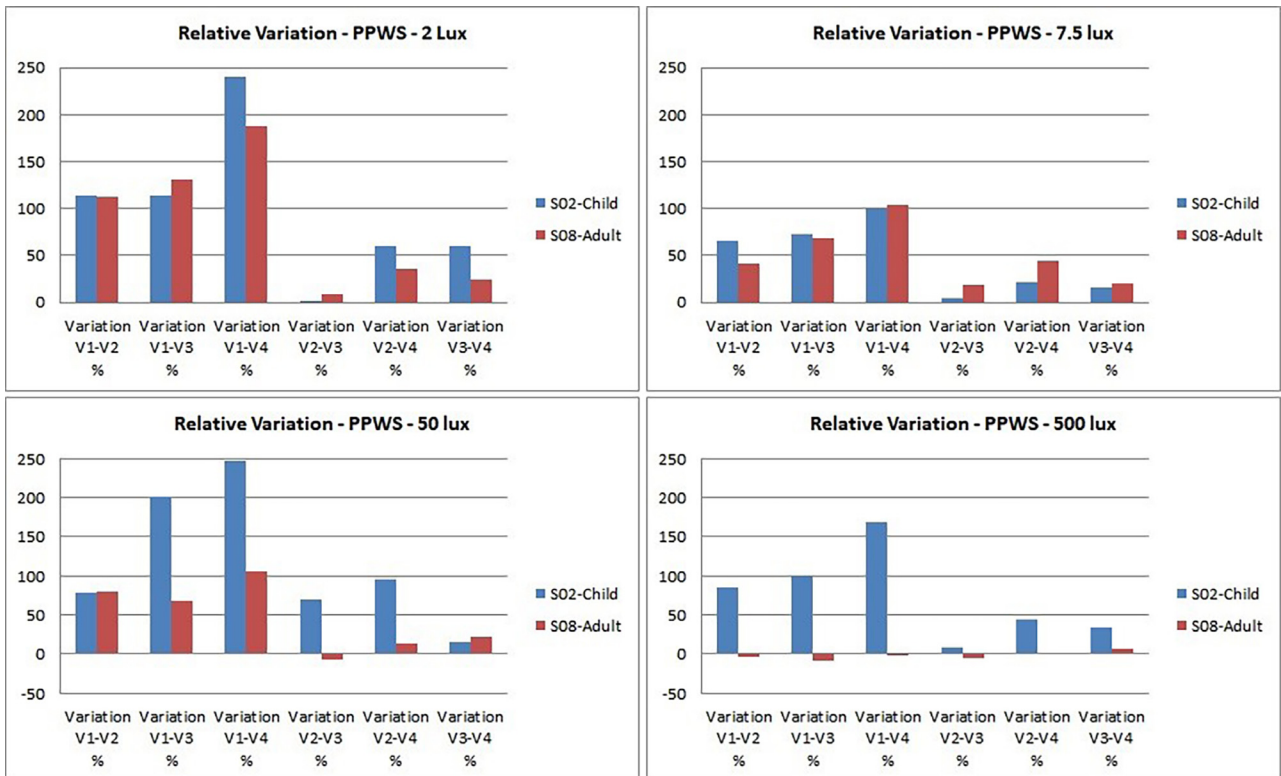


FIGURE 19. Relative variation for the percentage of preferred walking speed (PPWS) according to lighting conditions and visits. V = visit.

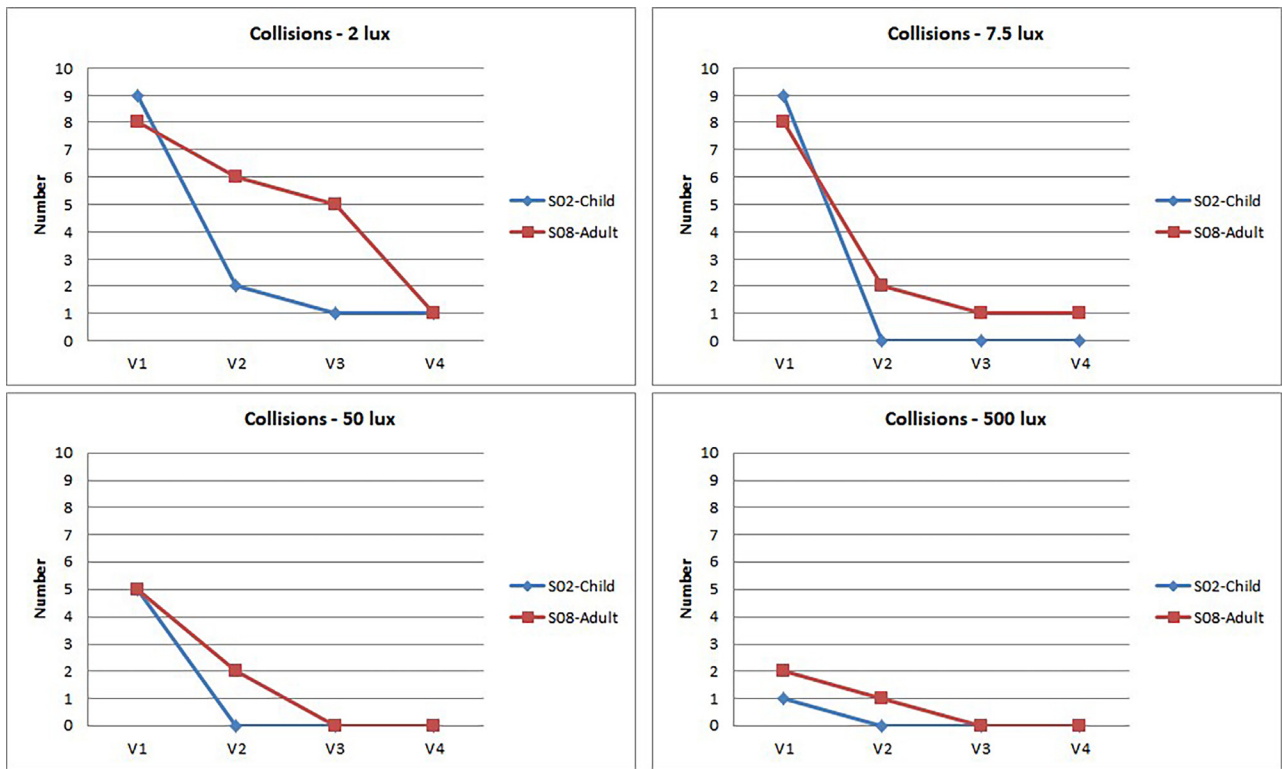


FIGURE 20. Evolution of collisions according to lighting conditions and visits. V = visit.

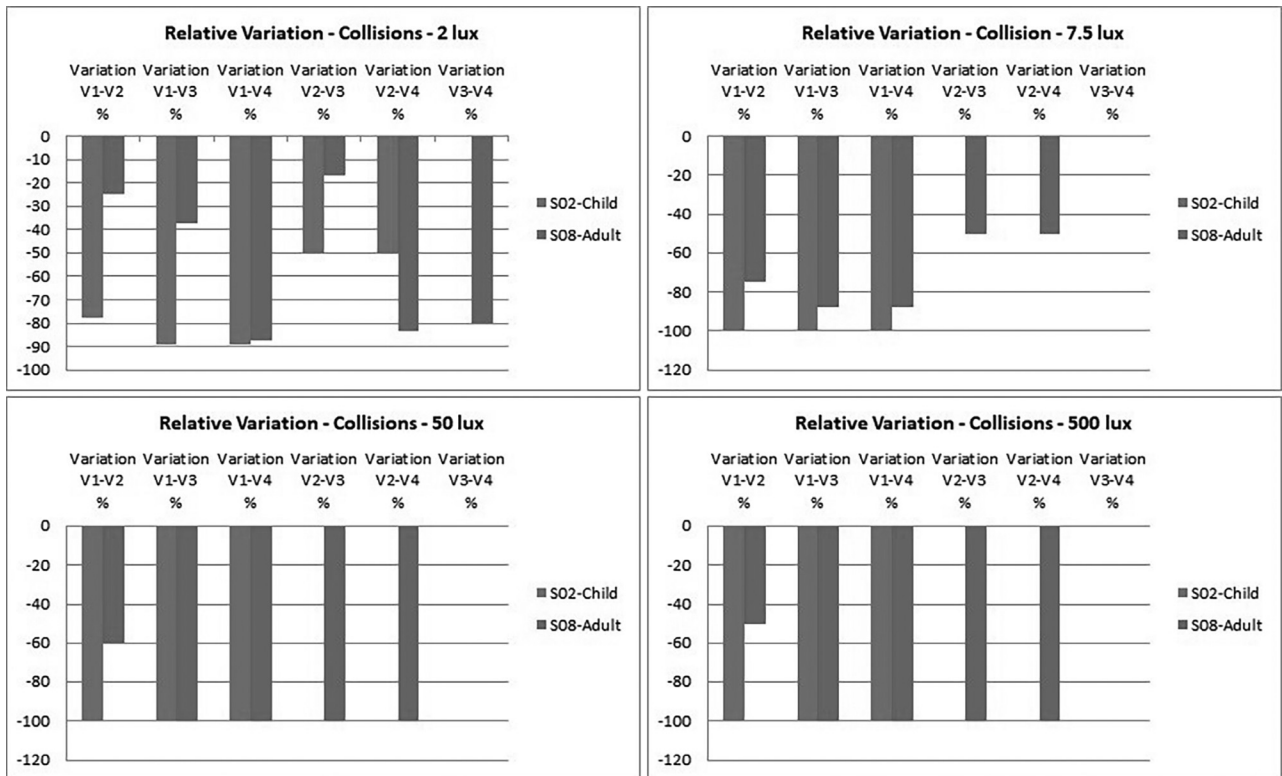


FIGURE 21. Relative variation for the percentage of preferred walking speed (PPWS) according to lighting conditions and visits. V = visit.

Thanks to further genetic research discoveries and advancements of the key DNA sequencing technologies, however, more than 300 retinal disease genes and loci have already been identified and/or mapped (<https://sph.uth.edu/retnet/>; last accessed on July 10, 2020), and more genes are yet to be identified, raising concerns about the feasibility to develop therapies that target every single gene defect causing IRD. Alongside this huge genetic heterogeneity and different modes of inheritance, other challenges are associated with the development of gene therapies for IRDs.

For IRDs caused by a single loss-of-function recessive gene defect, gene replacement therapy represents a powerful tool for correction of the genetic defect and restoration of the normal gene function. Based on better understanding of the retinal degeneration process and the encouraging results from the AAV-RPE65 gene replacement approach and its marketing approval, pioneering clinical studies were initiated to evaluate the safety and efficacy of gene therapy in other monogenic eye diseases, such as choroideremia (CHM) (NCT01461213, NCT02341807, NCT02077361, NCT02553135, NCT02671539, NCT02407678), X-linked retinoschisis (NCT02416622, NCT02317887), Usher syndrome (NCT01505062), ABCA4-associated Stargardt disease (NCT01367444), CNGA3-linked achromatopsia (NCT02610582, NCT02599922), MERTK-associated retinal disease (NCT01482195), and RPGR-associated RP (NCT03252847, NCT04312672, NCT03316560, NCT03316560, NCT04671433); and promising safety profiles were demonstrated from MERTK³² and CHM^{33,34} trials. In more detail, it has been demonstrated that retinal gene therapy can sustain and improve VA in a cohort of predominantly late-stage CHM patients,³⁵ and recovery of the retinal structure and function after treatment with adeno-associated virus (AAV) vector encoding Rab escort protein 1 was described.³⁶ The initial findings from a phase 1-2a open-label prospective clinical trial in 9 participants with pathogenic *RS1* mutations (X-linked retinoschisis) demonstrated that the gene therapy was generally well tolerated in the 3 dosage groups.³⁷ Similarly, the clinical trial evaluating the safety and efficacy of a single subretinal injection of rAAV.hCNGA3 to restore cone function in achromatopsia patients was reported.^{38,39}

Considering the difficulties in addressing the wide variety of already established and yet-to-be-established genetic, environmental, and lifestyle factors that contribute to IRDs, targeting a common, gene-independent mechanism would be a relevant therapeutic approach for a broad spectrum of retinal dystrophies.

Neuroprotection for rescuing cones

IRDs are often associated with an initial loss of rods, as the majority of mutations selectively affect rods. The loss of rods, however, is followed by a secondary degeneration of cones that occurs regardless of the underlying mutation. Since rod photoreceptors mediate night vision, whereas cones are used for daytime and color vision, one of our

core strategies consists in rescuing cones for saving daylight and high-acuity vision. As pointed out by Alan Wright:⁴⁰ “Paradoxically, in an age of artificial lighting we function very well without our rods, although they outnumber cones by twentyfold. ... Keep the cones alive and some 1.5 million people worldwide will see.”

For over two decades, our group has focused on deciphering the nature of interactions between the rods and the cones in the eye. Our group hypothesized and was the first to demonstrate that the normal retina releases a diffusible factor that helps cone cells to survive⁴¹ and that this retina-specific trophic factor, which we called rod-derived cone viability factor (RdCVF),⁴² not only induces cone survival in animal models of retinal degeneration but, more importantly, prevents both the shortening of the outer photoreceptor segment (that detects light) and the loss of function of cone photoreceptors.⁴³⁻⁴⁵ RdCVF is encoded by the *nucleoredoxin-like-1* gene (*NXNL1*). Next, we discovered the mechanism through which RdCVF promotes cone survival. The binding of RdCVF to the orphan cell surface receptor basigin—which is associated with the glucose transporter GLUT1—results in an accelerated glucose entry into cones and enhanced aerobic glycolysis.⁴⁶ In addition to RdCVF, *NXNL1* also encodes the thioredoxin enzyme rod-derived cone viability factor long (RdCVFL).⁴² We demonstrated that the administration of the enzymatically active RdCVFL to mice carrying a deletion of the *Nxnl1* gene reduces the damage produced by oxidative stress in cones.

Based on the demonstrated trophic interdependence of rods and cones, we hypothesize that a combinatory therapy of RdCVF and RdCVFL could be efficient in preventing secondary cone degeneration and saving central vision in patients with retinal dystrophies.⁴⁷ A single subretinal injection of a gene-based therapy with proprietary neurotrophic factors (code name SPVN06, SparingVision; European Orphan Designation granted on June 30, 2020) is currently in translation into a possible therapeutic agent to save cones and treat a spectrum of degenerative eye diseases.

Optogenetics for vision restoration

In advanced stages of retinal degeneration, when the outer photoreceptor segment is lost (resulting in lost photosensitivity), the cone bodies remain viable for extended periods of time.³⁻⁵ These “dormant” cones can potentially be reactivated by optogenetics, the techniques that makes cells light sensitive through expression of an “optogene” encoding light-gated channels or pumps. Optogenetics could also convert cells from the inner retinal neural layers (horizontal, bipolar, amacrine, and ganglion cells) into “artificial photoreceptors,” offering perspectives for vision restoration through artificially stimulated retinal activity that is gene independent and closer to the normal activity of retinal circuits. This hypothesis was tested by the group of Botond Roska at the Friedrich Miescher Institute, Basel, and our group (Picaud and Sahel at Institut de la Vision, Paris). Our collaborative research proved that in

animal models of advanced retinal degenerative disease, AAV-mediated delivery of the *NpHR* (halorhodopsin) gene into the surviving cone cell bodies of light-insensitive cones resulted in reactivated retinal ON and OFF pathways and visually guided behaviors, demonstrating a functional vision restoration.⁴ When targeted to human cone photoreceptors in ex vivo retinal explants with no intrinsic rod- or cone-mediated photosensitivity, NpHR was able to restore light responses,⁴ providing evidence for restored photosensitivity even in end-stage retinal degenerative diseases. These pioneering results opened new horizons for development of optogenetics as a potential vision restoration therapy. We specifically focused our research on development of viral vectors capable to carry the light-sensitive microbial opsins to a targeted population of anatomically preserved cells in the degenerating retina. We demonstrated efficient expression of optogenes in cones and retinal ganglion cells in nonhuman primate retinas in vivo and in human postmortem retinas in vitro.⁴⁸⁻⁵¹ Based on these results and the knowledge reported by other groups actively working in the field, we undertook translation of optogenetics-based gene therapy targeting the ganglion cells to the clinic for rescuing cone photoreceptors and secondary retinal neurons within the retinal network. A gene therapy product (GS030) encoding the red shifted channelrhodopsin variant ChrimsonR was produced by the French biotech company GenSight Biologics for delivery via the engineered AAV vector AAV2 7m8.⁵² This gene therapy, designed to confer a photoreceptive function to the preserved retinal ganglion cells, is supported with biomimetic goggles that capture visual information and amplify the light stimulation upon the transduced neuronal cells at the appropriate wavelength. A dose-escalation study (PIONEER; NCT03326336) was initiated to evaluate the safety and tolerability of GS030 in subjects with RP. Being independent of the genetic cause of the retinal dystrophy, the optogenetic approach can be applicable to a broad range of patients with rare genetic diseases of the retina (such as RP), as well as to more common retinal degenerative diseases, such as age-related macular degeneration.

In parallel to the optogenetic approach, retinal prostheses have the demonstrated ability to reactivate remaining retinal circuits at the level of bipolar or ganglion cells after photoreceptor loss. We have been involved in both the validation and registration of the Argus II prosthesis and in the preclinical/clinical development of PRIMA, as described below. Both epiretinal (Argus II; Second Sight Medical Products) and subretinal (Alpha IMS; Retina Implant AG) implants were proved to restore partial vision in blind people with IRDs.^{13,53} They have both received market approval in Europe and in the United States, but their production was suspended in 2019. Wireless subretinal prosthesis PRIMA (Pixium Vision) is currently under clinical evaluation in France and the United States (NCT03333954, NCT03392324). The appliance is characterized by photovoltaic electrodes with their own local return circuit

and independent function (potentially giving higher resolution) and a more simple surgical procedure. The first-in-human clinical trial to test the safety and efficacy of the prosthesis in patients with geographic atrophy (a late stage of dry age-related macular degeneration) demonstrated restored visual sensitivity in the former scotoma in all 5 study participants. In 3 of the patients, the proper placement of the chip allowed prosthetic VA of only 10%-30% less than the level expected from the pixel pitch (20/420).⁵⁴

Once the strategies described above become available, the decision to apply any of these will be based on a careful assessment of the status of the patient's retina and of the patient's needs and wishes.

• STRUCTURE-FUNCTION CROSS-SECTIONAL STUDIES:

The results of the cross-sectional transversal study analyzed the correlations between the structural data (from FAF imaging and OCT examinations) and functional variables. We observed that VA and MS are not strongly correlated with structural variables and have a weak discrimination power. When the anatomic-functional correlation coefficient is low ($r \leq 0.36$), the functional variables distinguish only poorly proportioned categories for the anatomic variable.

Moreover, despite a good correlation coefficient, the variable "VA" is still a poor discriminant. When we apply a decision tree in our cohort, we often find that the majority of patients are classified in a group of more than 110 patients with a median VA equal to 0.80. This is related to the fact that during the course of the disease, the patients keep their VA for a long time (in our cohort, there are 105 patients with a VA between 0.63 and 1.25 and 136 patients with a VA ≥ 0.50).

For the majority of the variables, functional impairment is greater when the anatomic variables are reduced, except the thickness of the widths of the ring of increased autofluorescence (HAFh and HAFv), which are more important when the functional variables are more altered. Thus, the increase in the thickness of the ring can be presented as a criterion for the severity of the functional impairment.

Our results are consistent with data from the literature showing a decrease in OCT and FAF variables, and with functional data. The decrease in retinal thickness is related to a decrease in VA.⁵⁵⁻⁵⁷

Regarding MS, its alteration is linked to the thinning of the retina and in particular the outer layers.⁵⁸⁻⁶⁰ Moon and associates⁶⁰ noted a link between the degradation of MS and the decrease in the central retina over an area of 3 mm around the fovea (corresponding to our variables "OCT_Ep_0-1" and "OCT_Ep_1-3").

When we divided the population into groups according to functional impairment in relation to VA or MS scores, it appeared that the criteria showing a real difference between all the groups are the internal horizontal and vertical diameters of HAF ring (FAF_GAH and FAF_GAV), the horizontal and vertical lengths of the ellipsoid zone

(OCT_EZh and OCT_EZv) and of the external limiting membrane (OCT_ELMh and OCT_ELMv), and the foveal thickness (OCT_Ep_0-1). The cross-correlation of the VA and MS groups is also very informative. At the less advanced stages of RP, VA is a poor discriminator. In the groups where the VA is greater than 0.3, almost all the variables are significantly different between the subgroups of MS, so retinal sensitivity becomes the criterion that can determine the severity of the disease. Furthermore, when the VA is inferior or equal to 0.3, the functional impairment is such that it persists only in patients with advanced disease ($MS \leq 20$ dB). Thus, the subgroups of different MS make it possible to distinguish patients with foveal involvement whose changing criteria are the central thickness of the retina (“OCT_Ep_0-1”) and the foveal sensitivity (CS). In the groups determined by the MS score, the VA appears to be discriminating, especially when the impairment is more important ($MS \leq 10$ dB). Indeed, we then distinguish statistically significant differences for most of the variables between the distinct VA subgroups.

The retrospective study has shown that the dimensions of the retina delimited by the ring of increased FAF (FAF_ACI) is the variable that evolves the most and the fastest in our cohort of RP patients. We calculated an annual progression (reduction) rate of -6.28% , closely followed by the variables FAF_GAH (-4.33%), FAF_GAV (-4.15%), OCT_EZh (-4.25%), and OCT_EZv (-4.27%). These results are of the same order of magnitude as the study by Sujirakul and associates (ref. 67) comparing the annual reduction rates of the ellipsoid zone and the horizontal and vertical diameters of the HAF ring. However, the latter showed a greater reduction of the ellipsoid zone ($4.9\%/y$) than the horizontal ($4.1\%/y$) and vertical ($4\%/y$) diameters of the HAF ring.

As observed in previous studies,^{60,61} our results also show a change in the structural variables following an exponential curve. The more advanced the disease stage, the less the variables change.

In their study, Aizawa and associates were able to correlate FAF and OCT data to functional data.⁵⁵ They find a significant link between the constriction of the FAF ring and the decrease in retinal sensitivity ($P = .0047$), VA loss ($P = .026$), and the decrease in the length of the ellipsoid zone ($P = .018$). In our study, the correlation between the changes of structural and functional variables was not demonstrated. However, the deterioration of the variable “macular sensitivity” (MS) appeared to be significantly related to the alteration of the variable “foveal sensitivity” (CS) ($r = 0.54$). In addition, we find a correlation between the constriction of the ring (reduction of the area of the internal circle of the HAF ring) and the degradation of the horizontal and vertical ellipsoid zone, with a correlation coefficient of $r = 0.57$ and $r = 0.54$, respectively. The decrease in the diameter of the ring represented by our variable “FAF_GAH” is also correlated with ellipsoid areas

($r = 0.84$ for “FAF_EZv” and $r = 0.75$ for “FAF_EZv”) as in the study by Aizawa and associates.⁵⁵

In our study, the disease progression appears to be the same in the right and left eyes for all of the variables tested. Some authors have concluded the same symmetrical disease progression,⁶² while others highlighted differences between the two eyes.⁶³⁻⁶⁵ It was reported that in a population with Usher syndrome, anatomic and functional variables were affected differently depending on the eye. Aizawa and associates⁶⁶ also found an asymmetry between the right and left eyes, with no significant correlation between the two eyes,^{55,67} identifying 19% of patients whose annual rate of progression of the ellipsoid zone is different according to the eyes. Thus, a difference between the right and left eyes could exist, at least for a minority of patients, so this must be taken into consideration—in particular during clinical trials when one eye receives the tested treatment and the contralateral eye is chosen as a control.

Directly imaging photoreceptors

In a normal eye, identifying cones by AO imaging is straightforward, because photoreceptor outer segments are the most reflective structures of the fundus. In fact, ballistic reflectance of photoreceptors accounts for a significant proportion of the brightness of the fundus in non-AO imaging systems. This has made AO-enhanced fundus imaging popular among the scientific community; however, pathologic retinas show many profound changes in their optical properties that alter the contrast of cones over the background. This translates in AO imaging to a generally dimmer contrast of altered cones. The only exception to this is the presence of “brilliant cones” and visibility of cones in the fovea. This, together with the rather poor robustness of AO to loss of transparency of ocular milieu, hampered the routine use of photoreceptor imaging for evaluating the progress of photoreceptor degeneration. Indeed, OCT is not only more robust than AOO, it is also capable of providing “internal quality control” of images because the intensity of the brightness (or the loss of brightness) can be conveniently normalized against the other structures.

Interpreting the images of damaged photoreceptors raises the issue of the actual correspondence with photoreceptors. This raises the issue of the reliability of automated cone-counting procedures. Human supervision may correct obvious artifacts, yet the sole presence of a white pixel is not enough to adjudicate it as a photoreceptor. It is well known that structures other than outer segments may mimic a cone-like mosaic such as hyperreflective punctuate patterns seen within areas of geographic atrophy,⁶⁸ which are thought to originate from the Bruch membrane. Hence, combining several imaging approaches, such as split detection and OCT, diminishes the risk of misinterpretations. Detecting directional variability may also contribute to identification of wave-guiding structures, which in the outer retina are most likely outer segments. However, a

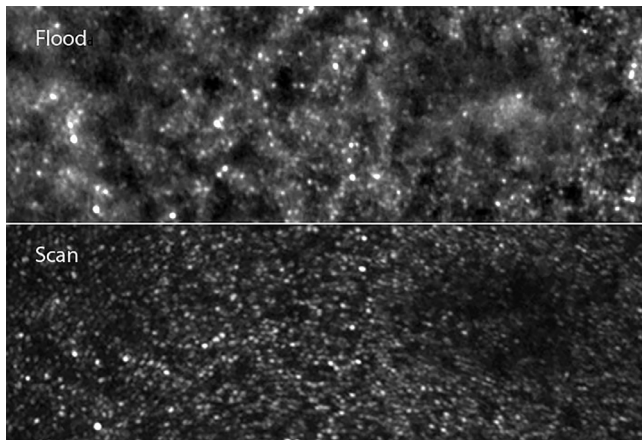


FIGURE 22. Comparison of flood adaptive optics-enhanced ophthalmoscopy (AOO) (Top) and scan AOO (Bottom). The fovea is on the right. Note the more regular aspect of the cone mosaic using scan AOO, but also the identification of additional disease features by flood AOO, such as brilliant central cones.

characterization of the angle-response curve is needed to use the Stiles-Crawford effect in clinical routine.

The correspondence between flood and scan imaging is therefore of potentially high interest. A comparison of flood vs scan AOO is shown in Figure 22.

Further evaluation of the function of these cones and the correspondence with their phenotypes could be of interest to investigate, in particular via optoretinography approaches such as intrinsic signal detection⁶⁹ or light-evoked changes in outer segment length.⁷⁰

- **ASSESSING FUNCTIONAL VISION:** In this first case study, we compared mobility performance in 17 RP vs 10 fully sighted subjects—nonmatched for sex and age—under different levels of illumination (235 lux, 1 lux, and 2 lux) through a performance-based test.

Our results confirm that RP is associated with decreased mobility performance. They are consistent with previous studies^{71,14,21} showing a reduced PPWS and greater number of collisions with obstacles in RP vs normally sighted controls. Increased WIT and number of course segments in low illumination may reflect a deteriorated fluidity of movement in subjects with RP. Psychological factors may partly explain these findings,^{21,72} as individual reactions to perceived danger may affect course management.

In the RP group, illumination level had a significant impact on all mobility parameters, except for PWS. PPWS decreased by nearly 50% at 1 and 2 lux vs 235 lux; WIT and number of course segments increased 2- or 3-fold, and the number of collisions up to 6-fold. The best mobility performance results were recorded at 235 lux in all RP subjects.

A larger PPWS decrease was reported in one RP study.⁷² Haymes and associates⁷² also reported a significant reduced PPWS with decreasing retinal illumination in a group of subjects with a 6-degree simulated VF. Their PPWS

averaged around 60%, whereas it was on average around 33% in our study. This difference may be related to the limited complexity of their outdoor mobility course, as PPWS significantly decreases if there are more pedestrians and obstacles.⁷³ Black and associates²¹ similarly found a reduction of PPWS for their RP group, but the value of PPWS reached 45% despite a course with more obstacles on the trajectory than ours, as well as luminance changes. Furthermore, this difference is probably not explained by the VF of the recruited subjects, which was similar in the two studies. However, it may be due to the extreme illumination values chosen in our study—1 and 2 lux—which probably created more difficulties than the 25 lux that they chose for their work.

We observed more mobility incidents in the RP group in low illumination, in line with prior findings in RP or low vision.^{21,14,71-75} However, the collision rate did not increase with smaller residual VF. This counterintuitive observation supports the assumption that RP subjects at the tubular vision stage may progressively develop adaptive skills to compensate for VF contraction.⁷⁶

We analyzed the relationship between clinical vision data and mobility performance under the different lighting conditions. In the literature, no visual variables are clearly identified to explain variations in performance. Our results showed that VF, VA, CS, and DA were correlated with mobility performance, but with different predictive values depending on the mobility variable and illumination level.

As anticipated, VF and CS were the best mobility performance predictors both in photopic and mesopic conditions, although this was not the case for PPWS. Similar results were noted in RP and low-vision groups in photopic conditions.^{74,77-79}

VA could also play a significant role in mobility performance, as previously demonstrated in RP mobility research,^{21,71,73,76-79} but with a lower predictive value than VF or CS.

PPWS variance is explained by VA, CS, and/or VF, both in photopic and in mesopic conditions in past research.^{21,72,73,76,79} In this study, VF explained the greater part of PPWS variance, except in mesopic conditions (in transition and after adaptation), when DA prevailed as the best predictor. Defective DA of photoreceptors seems to have a greater impact on walking than other visual parameters. Rod degeneration is expected to alter DA thresholds in RP (as rods are sensitive to low light conditions and ensure adaptation to darkness), while cone adaptation should be preserved. Our results suggest that cone adaptation impairment may occur, as results markedly differed between RP and control subjects at the 1-minute threshold associated with the light transition situation.

Previous research suggests that VA and CS accounted for part of the mobility performance variance only when measured in the actual test conditions (outdoors).⁷³ Further research is warranted with VA, VF, and CS measures in low illumination to confirm that DA is the best predictor

of PPWS under low illumination. If so, routinely including a DA test may limit the number of visual assessments required in standard and experimental conditions.

Mobility performance did not notably differ between 1 and 2 lux in the RP group. If the difference between these two illuminations is visually detectable by a healthy eye, they are probably too close to each other to be distinguished by a visually impaired person. A future objective would be to repeat these same mobility tests with a wider range of lighting conditions.

Subjects with RP typically encounter difficulties moving around in shifting light conditions. To the best of our knowledge, the correlation between DA thresholds and mobility performance had not been investigated prior to this study.

Our results suggest that including DA in the standard visual test panel may provide valuable information to better evaluate the relationship between clinical data and mobility performance in RP. DA may also serve to better evaluate the potential benefit of novel treatments in other ocular diseases affecting mobility performance.

In the second case study, we presented the results of two patients (1 child and 1 adult) treated with Luxturna[®]. They made four visits (visit 1, before treatment; visit 2, 1 month after treatment; visit 3, 3 months after treatment; and visit 4, and 6 months after treatment), during which they took part in visual examinations (VA, VF, FST, and OCT) and mobility courses with obstacles in the Streetlab artificial street under four lighting conditions (2 lux, 7.5 lux, 50 lux, and 500 lux).

We showed that Luxturna[®] had a very favorable impact on mobility performance—especially in low luminance (2 lux, 7.5 lux, and 50 lux)—still observable 6 months following the injection. The PPWS improved over time, with the largest relative variation being between visit 1 (before treatment) and visit 4 (6 months after injection). Objectively as well as subjectively, patients felt much more comfortable doing the mobility courses. Where they moved slowly and hit obstacles because they could not distinguish certain elements—particularly those with little contrast—on the path with low or even high luminance before treatment, they moved much more confidently 1 month after the injection.

The most spectacular progress was observed in the child's performance, in terms of both travel speed and reduction in the number of collisions. Nevertheless, the improvement in performance is also noticeable in the adult.

The results of this case study remain to be confirmed with other subjects and robust statistical analyses. It will be necessary to pay particular attention to the progress observed between visits 2 and 4 and make sure that it is not due to a learning effect.

From assessment of execution capacity to performance measurement

When aiming at determining therapeutic efficacy or describing the natural history of a pathology, one aspires to

measure the ability of patients to perform a task that is typical of daily life activities—for example, going out to buy bread down the street. We want to know, at the very least, if the patient is able to do it. In order to objectify this ability, it is necessary to set up experimental conditions reproducing the constraints of real life. In the given example, the patient needs to exit their apartment; locate the light switch in the corridor of the building, perhaps moving down the poorly lit stairs; exit the building; locate the bakery; walk on the sidewalk, avoiding collisions with fixed or mobile obstacles; and enter the bakery. This nonexhaustive set of subtasks cannot be easily tested in a single laboratory experiment.

However, involving the patient in a subtask is sufficient to determine their ability to perform it. Are they able to locate the switch in low light conditions or not? In fact, they may be able to do so in seconds and effortlessly, or by repeating the task multiple times. Ability or inability is not enough to appreciate the patient's difficulties. It is then essential to introduce a new variable: objective performance. Famose⁸⁰ defines performance in the context of physical and sporting activities as “the result obtained by a practitioner during the accomplishment of a given task, and perceived, measured and evaluated by him or by an outside observer.” In this case, the result of the execution of a task will be placed by the experimenter “on an evaluative continuum and compared to others.” It is safe to say that the performance depends on multiple variables. Here, performance is therefore conceived as a combination of discrete or continuous random variables (and covariant), whose result (or score) is placed on an evaluation scale and compared to others.

The need for multiple variables to measure performance

The observable parameters considered, or “outcome measures,” have yet to be determined. Of course, they strongly depend upon the task to carry out. An exhaustive list will not be drawn up here, as such lists are available in the literature.⁸¹ The usual variables are mostly either characteristics of the speed at which the task is performed (duration, and walking speed [often normalized to preferred walking speed] or precision variables (obstacle contacts, deviation from an optimal path). In general, precision variables make it easier to discriminate between normally sighted participants and patients with a visual impairment than do speed variables,^{82,14} although this is not always the case.⁸³ Combining accuracy and speed into a single variable makes the results even more predictive.⁸²

This finding is not surprising, and is often noted in motor control. For example, Fitts' law (1954),⁸⁴ widely used in human-computer interaction, predicts the accuracy of hand pointing according to the precision required by the target to be reached. This is commonly referred to as the speed-precision conflict. Mobility tasks in general, and obstacle courses in particular, are not immune from this conflict. The faster a participant moves, the more likely they are to hit obstacles.

Performance, now expressed as a score to be determined, should therefore be at least a function of time (or speed) of execution and accuracy, which may itself be a function of several other variables. In any case, these variables should be detailed as much as possible as measurable values defined within an interval (hypothesized notably from the literature), taking into account the unavoidable experimental limitations (i.e., too many variables could not be tested because their combinatorial mixing would be technically unattainable).

What are the constraints for creating a performance-based test?

In this section, we will present some principles to be taken into account for the design of a performance-based test (PBT). This work is not meant to be fully comprehensive and refers to specific readings⁸⁵ and FDA Guidance, 2019: <https://www.fda.gov/drugs/development-approval-process-drugs/public-workshop-patient-focused-drug-development-guidance-4-incorporating-clinical-outcome>.

The very first step consists of a qualitative parameterization of the test. Behavioral tasks must be designed based on the difficulties reported by patients in their daily life. Patient-reported outcomes can be used, such as quality-of-life questionnaires. At this stage, a precise characterization of the target population of the study is necessary. Indeed, it is not straightforward, based on a single test, to characterize patients over a broad spectrum of disease progression stages (i.e., patients at very early stages and even in very low vision).

It is then essential to quantitatively parameterize the test; that is, to define the complete and finite set of variables to be measured, as well as their limits and precision scale. The precision scale depends both on the relevance of the precision itself (for example, a measure of duration to the nearest second) and on technical considerations such as the resolution of the measuring instruments that are used.

The full test parameterization should maximize the capacity of discrimination between control subjects and patients (at an early stage of the disease, for example). Indeed, a participant who would be able to perform a task without difficulty might not attempt to move at his or her maximum speed. Therefore, performative conditions should be imposed on participants, based on the extreme values of the measured performance variables. Participants should be informed of the performance criteria considered via the instructions given at the beginning of the test (e.g., “you shall go as fast as possible without ever touching an object”).

The level of difficulty of the task should be high enough, or at least some variables manipulated in the experiment should allow control of the difficulty (such as the level of brightness), to classify and discriminate more easily between participating patients.

It is essential to control for learning effects, the best method being to ensure a sufficiently long learning period at the beginning of the test.

It is also important to define a difficulty metric for the task, associated with a visual parameter that has been affected by retinal disease. In the case of retinal dystrophies, this is typically related to the patient’s performance in perceiving contrasts in the darkness, but it could be acuity, VF size, a combination of both, or any other visual test result.

Finally, the construction of PBT requires the validation of the following criteria (FDA Guidance, 2018; <https://www.fda.gov/drugs/news-events-human-drugs/patient-focused-drug-development-guidance-methods-identify-what-important-patients-and-select>):

- (1) Construct validity. The construct validity of a test is the idea that the test measures what it intends to measure. A test is valid in this way if it allows differentiation among clinically distinct groups (eg, visually impaired vs controls).
- (2) Reliability. Reliability encompasses reproducibility and robustness. It means that scores should be reliable in test-retest, and between raters/ graders, and that its formulation does not depend on the framework (eg, the version of the operating system of the computer or the operability of the software).
- (3) Content validity. “The extent to which the [test] measures the concept of interest including evidence that the items and domains are appropriate and comprehensive relative to its intended measurement concept(s), population, and use.” A basic example of content validity is the representativity of some aspects of visual function.
- (4) Sensitivity to change (sometimes called responsiveness or ability to detect changes). This parameter can be characterized either in natural history studies, by an equivalent decrease in score and an aspect of visual function (VF, for example); or in a drug trial, by a similar increase.

It should be kept in mind that validation of a test is not possible in an absolute way—it is a cross-validation with other parameters. However, if the discriminating power of a test score (construct validity) is assessed by correlating it with clinical variables (such as acuity, VF, CS, anatomic data), the problem is somehow circular, because a PBT is designed to measure what usual clinical data, or quality-of-life questionnaires, do not accurately evaluate. Of course, it must be shown that it is possible to differentiate patients from normally sighted participants, or patients from each other at different stages of the disease (early vs. advanced), but the aim of this study is not to demonstrate a perfect correlation.

Moreover, numerous parameters, in addition to visual data, are involved in participants’ performance, such as coping strategies.

Taking into account patients' coping strategies—Towards a new score?

Despite the progression of the disease, from loss of photoreceptors to decreased visual function, some patients are able to adapt their behavior and adopt sensorimotor strategies. They may develop an adaptive gaze strategy to optimize visual sampling to maintain a sufficient performance in a task.⁸⁶

The implementation of these strategies, which can be different between patients, will be a source of variability in the score, and will impact the sensitivity to change and the validity of the test.

Several parameters can influence inter-subject variability:

- (1) Psychological factors. The level of acceptance of visual impairment by patients is a good example. Some patients in advanced stages of the disease consider themselves blind already, and are more susceptible to accept assistance/assistive devices such as a white cane, while others, more resilient, try to carry out most daily-life tasks independently. The latter are likely to perform better in PBTs. One must also consider the level of self-inhibition of patients, which, if important, leads them to consider that they are no longer able to perform a task—when this is not necessarily the case—and therefore they are less inclined to try to perform a task in a very difficult though possible condition.
- (2) Evolution of the disease. The time from onset of the disease, or rather the determination of how long the vision remained stable, is also an important source of variability. A patient who has recently lost a large part of his or her VF has a much lower probability to adopt strategies to compensate for the difficulties, at least partially.
- (3) Age. Age is of course a parameter that plays an important role in all aspects of PBT. It is probable that a young subject is likely to implement a coping strategy more quickly than an older subject.
- (4) The type of set-up strategies. The strategies could be cognitive (for example, a better memorization strategy) or sensorimotor.

In order to level out the effect of these factors of variability, we propose to define an adaptation sub-score for which the performance score could be renormalized, or represent an additional score.

How to detect a functional strategy?

What is an efficient coping strategy? The answer is not obvious. An adaptation strategy is not necessarily functional, and does not always promote performance. For example, one way to try to compensate for the loss of peripheral VF would be to make shorter and more frequent fixations to better sample the visual space while walking.⁸⁶ But this behavior might conceal several contributing phenomena.

In addition, its result, the sequence of fixations (or scan-path), can very well be organized and advantageous, or on the contrary completely unstructured and inefficient.

We must first determine whether one strategy (or the organization of the sequence of fixations, for example) is more efficient than another. We propose the study of eye and head movements as a method to extract the patients' strategies from experimental data.

In a goal-oriented locomotion task for RP participants with a restricted VF, we highlighted some adaptive gaze strategies.⁸⁶ RP patients exhibited a 28% increase in saccade frequency, compared to normally sighted individuals. This saccade over-representation was mainly observed in saccades generating a postsaccadic fixation located beyond the limits of the patient's field of view before saccade initiation. It suggests an adaptive gaze strategy developed to optimize visual sampling in goal-oriented locomotion. Moreover, we observed proactive target selection, fixation patterns including downward fixations, and synergistic head movements allowing for a successful trajectory execution (meaning making no contact with obstacles and reaching the end of the path). However, we have not highlighted the extent to which the coping strategy can improve performance in a task.

Other work on patients with homonymous VF defects⁸⁷ highlighted the link between performance and adaptive strategies in the context of driving. The authors measured both driving ability and oculomotor behavior of patients. Their results show that patients with a high driving ability performed more glances toward the area of their VF defect than patients with low driving abilities. Even if the pathology is difficult to compare with RP, this method is promising here because it allows characterization of a functional behavioral adaptation.

Moreover, this approach should allow the study of potential conflicts between strategies and identification of those that promote performance and the counterproductive ones.

The performance score in the task could therefore be corrected by an adaptation score, which would allow (1) a better understanding of part of the variability due to the visual condition, and (2) discrimination between effects of adaptation in the event that a patient would make progress from one session to the other not because of the treatment, but because of their ability to better resort to their residual vision.

CONCLUSION

Patient-centered management of retinal degenerations requires a careful assessment of the structural and functional status of the retina in order to decide upon the optimal therapeutic strategy: gene correction, neuroprotection, cell reactivation by optogenetics, prosthetics, or stem cells. Of equal importance is the demonstration of a therapeutic ben-

efit that is significant in daily life—that is, a change in functional vision. Functional vision assessment relies upon the design, validation, and implementation of patient-reported outcomes, PBTs, and related protocols aiming at developing reliable, reproducible metrics of daily life–related activities, at home and in the workplace. From the reductionist cell-level assessment to the holistic behavioral assessment, a multiscale metrology is in development, of which we presented elements here, mostly focused on cross-sectional analyses. Studies to analyze the correlations and predictive values of investigations performed in the clinical setting, including electrophysiology and psychophysics, should help in defining the set of tests necessary and sufficient to guide decisions and demonstrate unequivocal benefits. At the clinical level, correlations between structural changes and visual function will need to be refined. Some of the vision function tests might be predictive of functional vision

performance (eg, adaptation to levels of light, VF, etc). Naturalistic environments provide the best quality of information on the impact of disease and therapies in daily living activities.

Other methodologies, such as qualitative research, rarely used in ophthalmology,⁸⁸ should enable patient feedback to be incorporated into the analysis. Our future research will adapt such methods and enable a better understanding of patients' feelings about their visual impairment and the future, the impact on their independence, and their ability to interact with health providers and services, as well as the influence of social determinants of health and of education. The importance of these cannot be overstated. Such knowledge should guide better therapeutic strategies, including rehabilitation, and reduce social exclusion and stigma, while helping patients to develop psychological resources and social engagement.

Funding/Support: Programme Investissements d'Avenir IHU FOReSIGHT (ANR-18-IAHU-01), Programme Investissements d'Avenir LabEx LIFE-SENSES (ANR-10-LABX-65), European Research Council (ERC) Synergy Grant "HELMHOLTZ", Foundation Fighting Blindness. Financial Disclosures: J.A.S.: patents and personal financial interests in Pixium Vision, GenSight Biologics, SparingVision, Prophesee, Chronolife, Tilak Healthcare, Vegavect, Newsight, Replay Therapeutics, SharpEye; S.M.S.: consultant for Pixium Vision, SparingVision, Novartis, StreetLab; I.A.: consultant for Novartis, Biogen, MeiraGTx, Roche (none of these activities have relevance for the data presented herein); a founder of Gamut Tx; T.L.: patents and personal financial interests in SparingVision; C.Z.: consultant for Novartis, which has no relation with the data presented herein; S.P.: consultant and personal financial interests for Pixium Vision, GenSight Biologics; D.D.: inventor on a patent of adeno-associated virus virions with variant capsid and methods of use thereof with royalties paid to Avalanche Biotech (WO2012145601 A2) and on pending patent applications on noninvasive methods to target cone photoreceptors (EP17306429.6 and EP17306430.4) licensed to Gamut Tx; founder and acting CEO of Gamut Tx; K.G.: a founder and acting CEO of SharpEye (this activity is not relevant to the data presented herein); M.P.: a founder of SharpEye (this activity is not relevant to the data presented herein). The following authors declare no competing interests: C.P., C.A., K.B., A.E.C.R., L.A., E.G., and K.M. All authors attest that they meet the current ICMJE criteria for authorship.

Acknowledgment: The authors would like to thank the teams of the Quinze Vingts National Ophthalmology Hospital Clinical Investigation Center, StreetLab, and "HELMHOLTZ" project.

REFERENCES

- Dryja TP, McGee TL, Reichel E, et al. A point mutation of the rhodopsin gene in one form of retinitis pigmentosa. *Nature*. 1990;343:364–366.
- Russell S, Bennett J, Wellman JA, et al. Efficacy and safety of voretigene neparovec (AAV2-hRPE65v2) in patients with RPE65-mediated inherited retinal dystrophy: A randomised, controlled, open-label, phase 3 trial. *Lancet*. 2017;390:849–860.
- Sahel JA, Marazova K, Audo I. Clinical characteristics and current therapies for inherited retinal degenerations. *Cold Spring Harb Perspect Med*. 2014;5.
- Busskamp V, Duebel J, Balya D, et al. Genetic reactivation of cone photoreceptors restores visual responses in retinitis pigmentosa. *Science*. 2010;329:413–417.
- Sahel JA, Bennett J, Roska B. Depicting brighter possibilities for treating blindness. *Sci Transl Med*. 2019;11.
- Roska B, Sahel JA. Restoring vision. *Nature*. 2018;557:359–367.
- Miller DT, Williams DR, Morris GM, Liang J. Images of cone photoreceptors in the living human eye. *Vision Res*. 1996;36:1067–1079.
- Fankhauser F, Niederer PF, Kwasniewska S, van der Zypen E. Supernormal vision, high-resolution retinal imaging, multi-photon imaging and nanosurgery of the cornea—A review. *Technol Health Care*. 2004;12:443–453.
- Stiles WS, Crawford BH. The luminous efficiency of rays entering the eye pupil at different points. *Proc R Soc Lond*. 1933;B 112:428–450.
- Westheimer G. Directional sensitivity of the retina: 75 years of Stiles-Crawford effect. *Proc Biol Sci*. 2008;275:2777–2786.
- Lujan BJ, Roorda A, Croskrey JA, et al. Directional optical coherence tomography provides accurate outer nuclear layer and Henle fiber layer measurements. *Retina*. 2015;35:1511–1520.
- Salmon AE, Cooper RF, Langlo CS, Baghaie A, Dubra A, Carroll J. An automated reference frame selection (ARFS) algorithm for cone imaging with adaptive optics scanning light ophthalmoscopy. *Transl Vis Sci Technol*. 2017;6:9.
- da Cruz L, Dorn JD, Humayun MS, et al. Five-year safety and performance results from the Argus II retinal prosthesis system clinical trial. *Ophthalmology*. 2016;123:2248–2254.
- Chung DC, McCague S, Yu ZF, et al. Novel mobility test to assess functional vision in patients with inherited retinal dystrophies. *Clin Exp Ophthalmol*. 2018;46:247–259.
- Lombardi M, Zenouda A, Azoulay-Sebban L, et al. Correlation between visual function and performance of simulated daily living activities in glaucomatous patients. *J Glaucoma*. 2018;27:1017–1024.

16. Azoulay-Sebban L, Zhao Z, Zenouda A, et al. Correlations between subjective evaluation of quality of life, visual field loss, and performance in simulated activities of daily living in glaucoma patients. *J Glaucoma*. 2020;29:970–974.
17. Becu M, Sheynikhovich D, Tatur G, et al. Age-related preference for geometric spatial cues during real-world navigation. *Nat Hum Behav*. 2020;4:88–99.
18. Agathos CP, Ramanoel S, Becu M, Bernardin D, Habas C, Arleo A. Postural control while walking interferes with spatial learning in older adults navigating in a real environment. *Front Aging Neurosci*. 2020;12.
19. Ramanoel S, York E, Le Petit M, Lagrene K, Habas C, Arleo A. Age-related differences in functional and structural connectivity in the spatial navigation brain network. *Front Neural Circuits*. 2019;13:69.
20. Ramanoel S, Durtteste M, Becu M, Habas C, Arleo A. Differential brain activity in regions linked to visuospatial processing during landmark-based navigation in young and healthy older adults. *Front Hum Neurosci*. 2020;14.
21. Black A, Lovie-Kitchin JE, Woods RL, Arnold N, Byrnes J, Murrish J. Mobility performance with retinitis pigmentosa. *Clin Exp Optom*. 1997;80:1–12.
22. Cornelissen FW, Bootsma A, Kooijman AC. Object perception by visually impaired people at different light levels. *Vision Res*. 1995;35:161–168.
23. Roman AJ, Cideciyan AV, Aleman TS, Jacobson SG. Full-field stimulus testing (FST) to quantify visual perception in severely blind candidates for treatment trials. *Physiol Meas*. 2007;28:N51–N56.
24. Murakami Y, Ikeda Y, Nakatake S, et al. Necrotic enlargement of cone photoreceptor cells and the release of high-mobility group box-1 in retinitis pigmentosa. *Cell Death Discov*. 2015;1:15058.
25. Scoles D, Sulai YN, Langlo CS, et al. In vivo imaging of human cone photoreceptor inner segments. *Invest Ophthalmol Vis Sci*. 2014;55:4244–4251.
26. Boileve A, Jozwiak M, Malka D, et al. Vision loss after chemotherapy: An irinotecan-induced retinopathy. *Eur J Cancer*. 2019;112:80–82.
27. Miloudi C, Rossant F, Bloch I, et al. The negative cone mosaic: A new manifestation of the optical Stiles-Crawford effect in normal eyes. *Invest Ophthalmol Vis Sci*. 2015;56:7043–7050.
28. Bottin C, Grieve K, Rossant F, Pedinielli A, Mrejen S, Paques M. Directional variability of fundus reflectance in acute macular neuroretinopathy: Evidence for a contribution of the Stiles-Crawford effect. *Retin Cases Brief Rep*. 2018;12(Suppl 1):S19–S24.
29. Rossi EA, Chiara M, Eandi CM, Snyder V, et al. A new method for visualizing drusen and their progression in adaptive optics ophthalmoscopy. *Invest Ophthalmol Vis Sci*. 2020;61:203.
30. Audo I, Bujakowska KM, Leveillard T, et al. Development and application of a next-generation-sequencing (NGS) approach to detect known and novel gene defects underlying retinal diseases. *Orphanet J Rare Dis*. 2012;7:8.
31. Bennett J. Taking stock of retinal gene therapy: Looking back and moving forward. *Mol Ther*. 2017;25:1076–1094.
32. Ghazi NG, Abboud EB, Nowlaty SR, et al. Treatment of retinitis pigmentosa due to MERTK mutations by ocular subretinal injection of adeno-associated virus gene vector: Results of a phase I trial. *Hum Genet*. 2016;135:327–343.
33. MacLaren RE, Groppe M, Barnard AR, et al. Retinal gene therapy in patients with choroideremia: Initial findings from a phase 1/2 clinical trial. *Lancet*. 2014;383:1129–1137.
34. Edwards TL, Jolly JK, Groppe M, et al. Visual acuity after retinal gene therapy for choroideremia. *N Engl J Med*. 2016;374:1996–1998.
35. Xue K, Jolly JK, Barnard AR, et al. Beneficial effects on vision in patients undergoing retinal gene therapy for choroideremia. *Nat Med*. 2018;24:1507–1512.
36. Simunovic MP, Xue K, Jolly JK, MacLaren RE. Structural and functional recovery following limited iatrogenic macular detachment for retinal gene therapy. *JAMA Ophthalmol*. 2017;135:234–241.
37. Cukras C, Wiley HE, Jeffrey BG, et al. Retinal AAV8-RS1 gene therapy for X-linked retinoschisis: Initial findings from a phase I/IIa trial by intravitreal delivery. *Mol Ther*. 2018;26:2282–2294.
38. Kahle NA, Peters T, Zobor D, et al. Development of methodology and study protocol: Safety and efficacy of a single subretinal injection of rAAV.hCNGA3 in patients with CNGA3-linked achromatopsia investigated in an exploratory dose-escalation trial. *Hum Gene Ther Clin Dev*. 2018;29:121–131.
39. Fischer MD, Michalakis S, Wilhelm B, et al. Safety and vision outcomes of subretinal gene therapy targeting cone photoreceptors in achromatopsia: A nonrandomized controlled trial. *JAMA Ophthalmol*. 2020;138:643–651.
40. Wright AF. A searchlight through the fog. *Nat Genet*. 1997;17:132–134.
41. Mohand-Said S, Deudon-Combe A, Hicks D, et al. Normal retina releases a diffusible factor stimulating cone survival in the retinal degeneration mouse. *Proc Natl Acad Sci U S A*. 1998;95:8357–8362.
42. Leveillard T, Mohand-Said S, Lorentz O, et al. Identification and characterization of rod-derived cone viability factor. *Nat Genet*. 2004;36:755–759.
43. Mohand-Said S, Hicks D, Simonutti M, et al. Photoreceptor transplants increase host cone survival in the retinal degeneration (rd) mouse. *Ophthalmic Res*. 1997;29:290–297.
44. Yang Y, Mohand-Said S, Danan A, et al. Functional cone rescue by RdCVF protein in a dominant model of retinitis pigmentosa. *Mol Ther*. 2009;17:787–795.
45. Leveillard T, Sahel JA. Rod-derived cone viability factor for treating blinding diseases: From clinic to redox signaling. *Sci Transl Med*. 2010;2:26ps16.
46. Ait-Ali N, Fridlich R, Millet-Puel G, et al. Rod-derived cone viability factor promotes cone survival by stimulating aerobic glycolysis. *Cell*. 2015;161:817–832.
47. Mei X, Chaffiol A, Kole C, et al. The thioredoxin encoded by the rod-derived cone viability factor gene protects cone photoreceptors against oxidative stress. *Antioxid Redox Signal*. 2016;24:909–923.
48. Sengupta A, Chaffiol A, Mace E, et al. Red-shifted channelrhodopsin stimulation restores light responses in blind mice, macaque retina, and human retina. *EMBO Mol Med*. 2016;8:1248–1264.
49. Khabou H, Garita-Hernandez M, Chaffiol A, et al. Noninvasive gene delivery to foveal cones for vision restoration. *JCI Insight*. 2018;3.

50. Chaffiol A, Caplette R, Jaillard C, et al. A new promoter allows optogenetic vision restoration with enhanced sensitivity in macaque retina. *Mol Ther*. 2017;25:2546–2560.
51. Gauvain G, Akolkar H, Chaffiol A, et al. Optogenetic therapy: High spatiotemporal resolution and pattern discrimination compatible with vision restoration in non-human primates. *Communications Biology*. 2021;4:125.
52. Dalkara D, Byrne LC, Klimczak RR, et al. In vivo-directed evolution of a new adeno-associated virus for therapeutic outer retinal gene delivery from the vitreous. *Sci Transl Med*. 2013;5:189ra76.
53. Stingl K, Schippert R, Bartz-Schmidt KU, et al. Interim results of a multicenter trial with the new electronic subretinal implant Alpha AMS in 15 patients blind from inherited retinal degenerations. *Front Neurosci*. 2017;11:445.
54. Palanker D, Le Mer Y, Mohand-Said S, Muqit M, Sahel JA. Photovoltaic restoration of central vision in atrophic age-related macular degeneration. *Ophthalmology*. 2020;127:1097–1104.
55. Aizawa S, Mitamura Y, Baba T, Hagiwara A, Ogata K, Yamamoto S. Correlation between visual function and photoreceptor inner/outer segment junction in patients with retinitis pigmentosa. *Eye (Lond)*. 2009;23:304–308.
56. Yoon CK, Yu HG. The structure-function relationship between macular morphology and visual function analyzed by optical coherence tomography in retinitis pigmentosa. *J Ophthalmol*. 2013;2013.
57. Lupo S, Grenga PL, Vingolo EM. Fourier-domain optical coherence tomography and microperimetry findings in retinitis pigmentosa. *Am J Ophthalmol*. 2011;151:106–111.
58. Rangaswamy NV, Patel HM, Locke KG, Hood DC, Birch DG. A comparison of visual field sensitivity to photoreceptor thickness in retinitis pigmentosa. *Invest Ophthalmol Vis Sci*. 2010;51:4213–4219.
59. Lenassi E, Troeger E, Wilke R, Hawlina M. Correlation between macular morphology and sensitivity in patients with retinitis pigmentosa and hyperautofluorescent ring. *Invest Ophthalmol Vis Sci*. 2012;53:47–52.
60. Moon CH, Park TK, Ohn YH. Association between multifocal electroretinograms, optical coherence tomography and central visual sensitivity in advanced retinitis pigmentosa. *Doc Ophthalmol*. 2012;125:113–122.
61. Birch DG, Locke KG, Wen Y, Locke KI, Hoffman DR, Hood DC. Spectral-domain optical coherence tomography measures of outer segment layer progression in patients with X-linked retinitis pigmentosa. *JAMA Ophthalmol*. 2013;131:1143–1150.
62. Massof RW, Finkelstein D, Starr SJ, Kenyon KR, Fleischman JA, Maumenee IH. Bilateral symmetry of vision disorders in typical retinitis pigmentosa. *Br J Ophthalmol*. 1979;63:90–96.
63. Khateb S, Nassisi M, Bujakowska KM, et al. Longitudinal clinical follow-up and genetic spectrum of patients with rod-cone dystrophy associated with mutations in PDE6A and PDE6B. *JAMA Ophthalmol*. 2019;137:669–679.
64. Khateb S, Mohand-Said S, Nassisi M, et al. Phenotypic characteristics of rod-cone dystrophy associated with Myo7a mutations in a large French cohort. *Retina*. 2020;40:1603–1615.
65. Fakin A, Jarc-Vidmar M, Glavac D, Bonnet C, Petit C, Hawlina M. Fundus autofluorescence and optical coherence tomography in relation to visual function in Usher syndrome type 1 and 2. *Vision Res*. 2012;75:60–70.
66. Aizawa S, Mitamura Y, Hagiwara A, Sugawara T, Yamamoto S. Changes of fundus autofluorescence, photoreceptor inner and outer segment junction line, and visual function in patients with retinitis pigmentosa. *Clin Exp Ophthalmol*. 2010;38:597–604.
67. Sujirakul T, Lin MK, Duong J, Wei Y, Lopez-Pintado S, Tsang SH. Multimodal imaging of central retinal disease progression in a 2-year mean follow-up of retinitis pigmentosa. *Am J Ophthalmol*. 2015;160:786–798 e4.
68. Paques M, Meimon S, Rossant F, et al. Adaptive optics ophthalmoscopy: Application to age-related macular degeneration and vascular diseases. *Prog Retin Eye Res*. 2018;66:1–16.
69. Grieve K, Roorda A. Intrinsic signals from human cone photoreceptors. *Invest Ophthalmol Vis Sci*. 2008;49:713–719.
70. Azimipour M, Migacz JV, Zawadzki RJ, Werner JS, Jonnal RS. Functional retinal imaging using adaptive optics swept-source OCT at 1.6 MHz. *Optica*. 2019;6:300–303.
71. Geruschat DR, Turano KA, Stahl JW. Traditional measures of mobility performance and retinitis pigmentosa. *Optom Vis Sci*. 1998;75:525–537.
72. Haymes S, Guest D, Heyes A, Johnston A. Comparison of functional mobility performance with clinical vision measures in simulated retinitis pigmentosa. *Optom Vis Sci*. 1994;71:442–453.
73. Haymes S, Guest D, Heyes A, Johnston A. Mobility of people with retinitis pigmentosa as a function of vision and psychological variables. *Optom Vis Sci*. 1996;73:621–637.
74. Marron JA, Bailey IL. Visual factors and orientation-mobility performance. *Am J Optom Physiol Opt*. 1982;59:413–426.
75. Ivanov IV, Mackeben M, Vollmer A, Martus P, Nguyen NX, Trauzettel-Klosinski S. Eye movement training and suggested gaze strategies in tunnel vision - A randomized and controlled pilot study. *PLoS One*. 2016;11.
76. Alshaghthrah AM, Dickinson CM. A practical indoor mobility course to assess the functional effect of tunnel vision. *SJOVS*. 2014;7:1–7.
77. Velikay-Parel M, Ivastinovic D, Koch M, et al. Repeated mobility testing for later artificial visual function evaluation. *J Neural Eng*. 2007;4:S102–S107.
78. Finger RP, McSweeney SC, Deverell L, et al. Developing an instrumental activities of daily living tool as part of the low vision assessment of daily activities protocol. *Invest Ophthalmol Vis Sci*. 2014;55:8458–8466.
79. Finger RP, Ayton LN, Deverell L, et al. Developing a very low vision orientation and mobility test battery (O&M-VLV). *Optom Vis Sci*. 2016;93:1127–1136.
80. Famose JP. La performance motrice: Un essai de définition. *Cognition et performance* INSEP-Éditions Paris; 1993:21–40.
81. Chang KJ, Dillon LL, Deverell L, Boon MY, Keay L. Orientation and mobility outcome measures. *Clin Exp Optom*. 2020;103:434–448.
82. Warrian KJ, Katz LJ, Myers JS, et al. A comparison of methods used to evaluate mobility performance in the visually impaired. *Br J Ophthalmol*. 2015;99:113–118.
83. Kumaran N, Ali RR, Tyler NA, Bainbridge JWB, Michaelides M, Rubin GS. Validation of a vision-guided mobility assessment for RPE65-associated retinal dystrophy. *Transl Vis Sci Technol*. 2020;9:5.

84. Fitts PM. The information capacity of the human motor system in controlling the amplitude of movement. *J Exp Psychol.* 1954;47:381–391.
85. Warrian KJ, Altangerel U, Spaeth GL. Performance-based measures of visual function. *Surv Ophthalmol.* 2010;55:146–161.
86. Authie CN, Berthoz A, Sahel JA, Safran AB. Adaptive gaze strategies for locomotion with constricted visual field. *Front Hum Neurosci.* 2017;11:387.
87. Kasneci E, Sippel K, Aehling K, et al. Driving with binocular visual field loss? A study on a supervised on-road parcours with simultaneous eye and head tracking. *PLoS One.* 2014;9:e87470.
88. Bennion AE, Shaw RL, Gibson JM. What do we know about the experience of age related macular degeneration? A systematic review and meta-synthesis of qualitative research. *Soc Sci Med.* 2012;75:976–985.